Final Technical Report

June 23, 2016

Award Number: G14AP00030

Term Covered: March 2014 through February 2016

Earthquake Magnitude Estimation from Fault Dimensions and Slip Rate

John G. Anderson, Glenn P. Biasi & Steven G. Wesnousky

Nevada Seismological Laboratory
University of Nevada
Reno, Nevada 89557, United States

Report submitted: June 2016

Abstract

This study addresses whether knowing the geological slip rates on a fault improves estimates of magnitude (M_W) of shallow, surface-rupturing earthquakes. Based on 43 earthquakes from the database of Wells and Coppersmith (1994), Anderson et al. (1996) suggested that estimates of M_W from rupture length (L_E) are improved by incorporating the slip rate of the fault (S_F). We re-evaluate this relationship with an expanded database of 80 events, including 57 strike-slip, 12 reverse, and 11 normal faulting events. When the data are subdivided by fault mechanism, magnitude predictions from rupture length are improved for strike-slip faults, but not for reverse or normal faults. A linear model with $M_W \sim \log L_E$ over all rupture lengths implies that the stress drop is a strong function of the rupture length - an observation that is not supported by teleseismic observations. With a slight improvement in the quality of fit, we find a model with slope $2 \log L_E$ at low rupture length that transitions to a slope of $(2/3) \log L_E$ at high rupture length, and has constant stress drop over the entire range. The dependence on slip rate for strike-slip faults is a persistent feature of all considered models. The observations support the conclusion that for strike-slip faults, the static stress drop, on average, tends to decrease as the fault slip rate increases.

Fault Scaling Relationships Depend on the Average Geological Slip Rate

John G. Anderson, Glenn P. Biasi, Steven G. Wesnousky

1 Abstract

This study addresses whether knowing the geological slip rates on a fault improves estimates of magnitude (M_W) of shallow, surface-rupturing earthquakes. Based on 43 earthquakes from the database of Wells and Coppersmith (1994), Anderson et al. (1996) suggested that estimates of M_W from rupture length (L_E) are improved by incorporating the slip rate of the fault (S_F). We re-evaluate this relationship with an expanded database of 80 events, including 57 strike-slip, 12 reverse, and 11 normal faulting events. When the data are subdivided by fault mechanism, magnitude predictions from rupture length are improved for strike-slip faults, but not for reverse or normal faults. A linear model with $M_W \sim \log L_E$ over all rupture lengths implies that the stress drop is a strong function of the rupture length - an observation that is not supported by teleseismic observations. With a slight improvement in the quality of fit, we find a model with slope $2 \log L_E$ at low rupture length that transitions to a slope of $(2/3) \log L_E$ at high rupture length, and has constant stress drop over the entire range. The dependence on slip rate for strike-slip faults is a persistent feature of all considered models. The observations support the conclusion that for strike-slip faults, the static stress drop, on average, tends to decrease as the fault slip rate increases.

2 Introduction

Models for estimating the possible magnitude of an earthquake from geological observations of the fault length are an essential component of any state-of-the-art seismic hazard analysis. The input to either a probabilistic or deterministic seismic hazard analysis requires geological constraints because the duration of instrumental observations of seismicity are too short, by 1-2 orders of magnitude, to observe the size and estimate the occurrence rates of the largest earthquakes. Thus, wherever the rupture of past earthquakes remain visible in the geological record, or whenever a fault is well mapped, it is essential for the seismic hazard analysis to consider the hazard from that fault, and an estimate of the magnitude of the earthquake that might occur is an essential part of the process. The primary goal of this study is to determine if magnitude estimates can be improved by incorporating the geological slip rate of the fault. The effect of slip rate is tested against three model shapes for the scaling relationship to confirm if it is not an artifact of a particular assumption for how magnitude depends on

rupture length.

Numerous models for estimating magnitude from rupture length have been published. Early studies were by Tocher (1958) and Iida (1959). Wells and Coppersmith (1994) published an extensive scaling study based on 244 earthquakes. Some of the more recent studies include Anderson et al., (1996), Hanks and Bakun (2002, 2008), Shaw and Wesnousky (2008) and Leonard (2010, 2012, 2014). For probabilistic studies, and for earthquake source physics, it is valuable to try to reduce the uncertainty in these relations. Anderson et al. (1996) (hereafter abbreviated as ASW96) investigated whether the slip rate on a fault improves magnitude estimates given rupture length. The relationship that they found is $M_W = 5.12 + 1.16 \log L_E - 0.20 \log S_F$. Since publication of that report, the number of earthquakes with magnitude, rupture length, and slip rate estimates available has approximately doubled. This paper considers whether these new data improve their estimate.

One consideration in developing a scaling model is seismological observations that the stress drop in earthquakes is practically independent of magnitude. Kanamori and Anderson (1975) is one of the early papers to make this observation. Recent studies that have supported this result include Allman and Shearer (2009) and Baltay et al. (2011). As magnitude decreases, attenuation and decreasing stress drop have a similar effect on the spectral shape (e.g. Anderson, 1986), but studies that have taken considerable care to separate the effects have generally concluded that the stress drop remains independent of magnitude down to extremely small magnitudes (e.g. Abercrombie, 1995; Ide et al., 2003; Baltay et al., 2010, 2011). A caveat is that for any given fault dimension the range of magnitudes can vary considerably (e.g. Kanamori and Allen, 1986). In spite of this variability, it seems reasonable to evaluate whether a scaling relationship that is based on a constant stress drop can be proposed that performs well with the data for magnitude and rupture length. A discussion of models for the relationship of stress drop and the fault dimensions is deferred to an appendix. The following sections describe the data, fit some alternative models to the data, and discuss the results.

3 Data

Table 1 lists the earthquakes used in this analysis. A complete list of considered events is given in the spreadsheet *aMasterEventTable_2015-10-6b.xlsx*. This spreadsheet, together with citations for all values, is given in an Online Supplement. Events considered for analysis come from Biasi and Wesnousky (2016) and Anderson et al. (1996). Some events they considered were not included because they did not have surface rupture or because fault slip rate was not sufficiently well known. The events that are used are listed in Tables 1 and 2.

Figure 1 shows the cumulative number of earthquakes used as a function of time. From 1944-2013, the rate of usable events is relatively steady, about 0.9 events per year. The rate is lower prior to ~1930, reflecting the smaller fraction of well documented surface ruptures. Considering the frequency of usable events

in the most recent half century, Figure 1 suggests that there were potentially a few dozen earthquakes from the late 19th and early 20th century that might eventually be added in a future compilation.

The earthquakes were separated into general categories of strike-slip, normal, and reverse faulting. Figure 2 shows the exceedance rates of earthquakes in each of these categories as a function of magnitude, both combined and separated by focal mechanism. To estimate the rates, the number of earthquakes for each of the curves was divided by 100 years. Considering Figure 1, this is obviously an approximation, but the events prior to ~1910 may roughly compensate for the missing events since 1910, so we consider the result to be useful. For instance, Figure 2 finds that events that cause surface rupture with Mw>=7 have occurred roughly once every two years, that 80% of those events were strike slip, about 15% had reverse mechanisms, and about 5% had normal mechanisms. Anderson et al. (2005) previously estimated the relative rates of surface-rupturing events for purposes of assessing the rates at which strong motion data might be gathered from large crustal earthquakes. The assessment in Figure 2 updates those estimates.

Figure 3 shows maps with locations of all events, using different types of symbols for diffferent mechanisms. The insets shows more details on locations of events fom the western US, the eastern Mediterranean region, and Japan.

Table 1: Earthquakes from 1968-2011 used in this study.

Event Number	Event Name	Event Date	Mw	Rupture Length, km	Slip Rate, mm/yr
2	Fukushima-Hamadori, Japa	11-Apr-2011	6.7	15	0.02
4	Yushu, China	14-Apr-2010	6.8	52	12
5	El Mayor Cucapah	4-Apr-2010	7.3	117	2.5
6	Wenchuan, China	12-May-2008	7.9	240	1.3
7	Kashmir, Pakistan	8-Oct-2005	7.6	70	3.1
8	Chuya,Russia (Gorny Altay)	27-Sep-2003	7.2	70	0.5
9	Denali, Alaska	3-Nov-2002	7.8	340	12.4
10	Kunlun, China	14-Nov-2001	7.7	450	10
11	Duzce, Turkey	12-Nov-1999	7.1	40	15
12	Hector Mine, California	16-Oct-1999	7.1	48	0.6
13	Chi-Chi, Taiwan	21-Sep-1999	7.7	72	12.9
14	Izmit, Turkey	17-Aug-1999	7.5	145	12
15	Fandoqa, Iran	14-Mar-1998	6.6	22	2
16	Manyi, China	8-Nov-1997	7.4	170	3
17	Sakhalen Island (Neftegors	27-May-1995	7	40	4
18	Northridge	17-Jan-1994	6.7	21	0.4
19	Landers	28-Jun-1992	7.2	77	0.4
20	Luzon	16-Jul-1990	7.7	112	15
21	Rudbar	20-Jun-1990	7.4	80	1
22	Loma Prieta	17-Oct-1989	6.8	35	3.2
25	Superstition Hill	24-Nov-1987	6.6	25	3
26	Edgecumbe	2-Mar-1987	6.4	15.5	2
28	Marryat	3-Mar-1986	5.8	13	0.005
29	Morgan Hill	24-Apr-1984	6.1	20	5.2
30	Borah Peak	28-Oct-1983	6.8	36	0.15
31	Coalinga,	2-May-1983	6.4	25	1.4
32	Sirch	29-Jul-1981	7.1	65	4.3
33	Corinth	25-Feb-1981	6.1	14	1.7
34	Corinth	4-Mar-1981	5.9	15	0.3
35	Daofu	24-Jan-1981	6.7	44	12
36	El Asnam (Ech Cheliff)	10-Oct-1980	6.9	36	0.8
37	Imperial Valley,	15-Oct-1979	6.4	36	17
38	Coyote Lake,	6-Aug-1979	5.8	14	11.9
40	Tabas	16-Sep-1978	7.4	90	1.3
41	Bob-Tangol	19-Dec-1977	5.8	19.5	4
42	Motagua	4-Feb-1976	7.5	230	12
43	Luhuo	6-Feb-1973	7.5	90	14
44	San Fernando	9-Feb-1971	6.8	19	1.8
45	Tonghai	4-Jan-1970	7.2	60	2
46	Dasht-e-Bayaz	31-Aug-1968	7.1	80	5
47	Borrego Mntn	9-Apr-1968	6.6	33	6.7

Table 2: Earthquakes from 1848 - 1967 used in this study.

Event Number	Event Name	Event Date	Mw	Rupture Length, km	Slip Rate, mm/yr
48	Mudurnu Valley	22-Jul-1967	7.3	80	18
49	Parkfield	28-Jun-1966	6.2	28	30
51	Alake Lake - or - Tuosuohu Lake or Dulan	19-Apr-1963	7	40	12
52	Ipak or Buyin-Zara	1-Sep-1962	7	100	1
53	Hebgen Lake	18-Aug-1959	7.3	25	0.5
54	Gobi-Altai	4-Dec-1957	8.1	260	1
55	San Miguel	14-Feb-1956	6.6	20	0.3
56	Fairview Peak	16-Dec-1954	7.1	46	0.14
57	Dixie Valley	16-Dec-1954	6.6	47	0.5
58	Gonen-Yenice	18-Mar-1953	7.3	60	6.8
60	Gerede-Bolu	1-Feb-1944	7.3	155	18
61	Tosya	26-Nov-1943	7.6	275	19
62	Tottori	10-Sep-1943	6.9	33	0.3
63	Niksar-Erbaa	20-Dec-1942	6.8	50	19
64	Imperial Valley,	19-May-1940	7.1	60	17
65	Erzincan	25-Dec-1939	7.8	330	19
66	Tuosuo Lake - Huashixia	7-Jan-1937	7.6	150	11
67	Parkfield	8-Jun-1934	6.2	25	30
68	Long Beach	10-Mar-1933	6.4	22	1.1
69	Changma	25-Dec-1932	7.6	149	5
70	Fuyun	10-Aug-1931	7.9	160	0.3
71	N. Izu	25-Nov-1930	6.9	28	2.4
72	Laikipia	6-Jan-1928	6.8	38	0.18
73	Tango	7-Mar-1927	7	35	0.3
74	Luoho-Qiajiao(Daofu)	24-Mar-1923	7.3	80	10
75	Haiyuan	16-Dec-1920	8	237	7
76	Pleasant Valley	3-Oct-1915	7.3	61	0.1
77	Chon-Kemin (Kebin)	3-Jan-1911	8	177	2
78	San Francisco	18-Apr-1906	7.9	497	21
79	Bulnay	23-Jul-1905	8.5	375	3
80	Laguna Salada	1892-02-23	7.2	42	2.5
81	Rikuu	1896-08-31	7.2	40	1
82	Nobi/ Mino-Owari	28-Jun-1908	7.4	80	1.6
83	Canterbury	1888-09-01	7.1	65	14
84	Sonora	1887-05-13	7.2	101.8	0.08
85	Owens Valley	1872-03-26	7.4	110	3.5
86	Hayward	1868-10-21	6.9	61	8
87	Fort Tejon	1857-01-09	7.8	339	25
88	Marlborough	1848-10-16	7.5	134	5.6

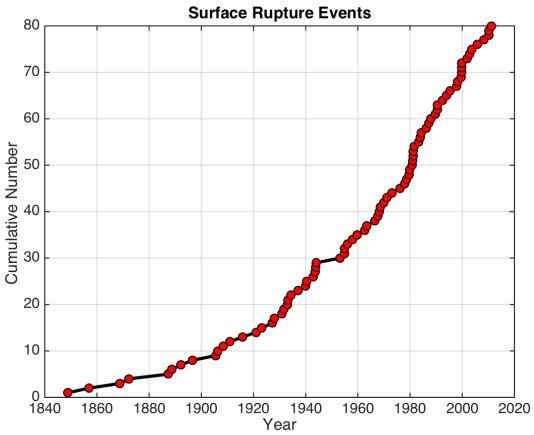

Figure 1: Cumulative number of events used in this analysis (Table 1 and 2), shown as a function of time.

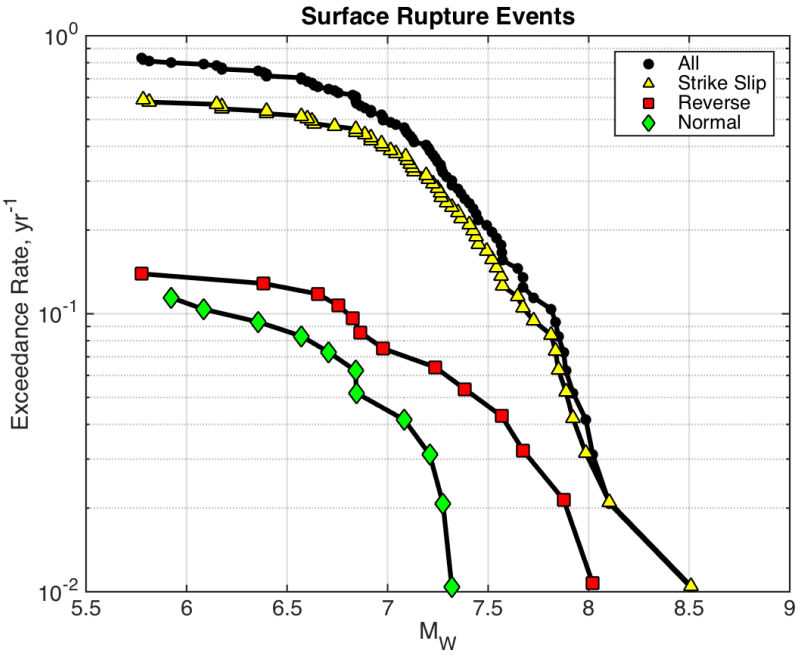

Figure 2: Event rates, as a function of magnitude and event types. The rates are estimated based on the approximation that the data represent about 100 years of seismicity, as discussed in the text.

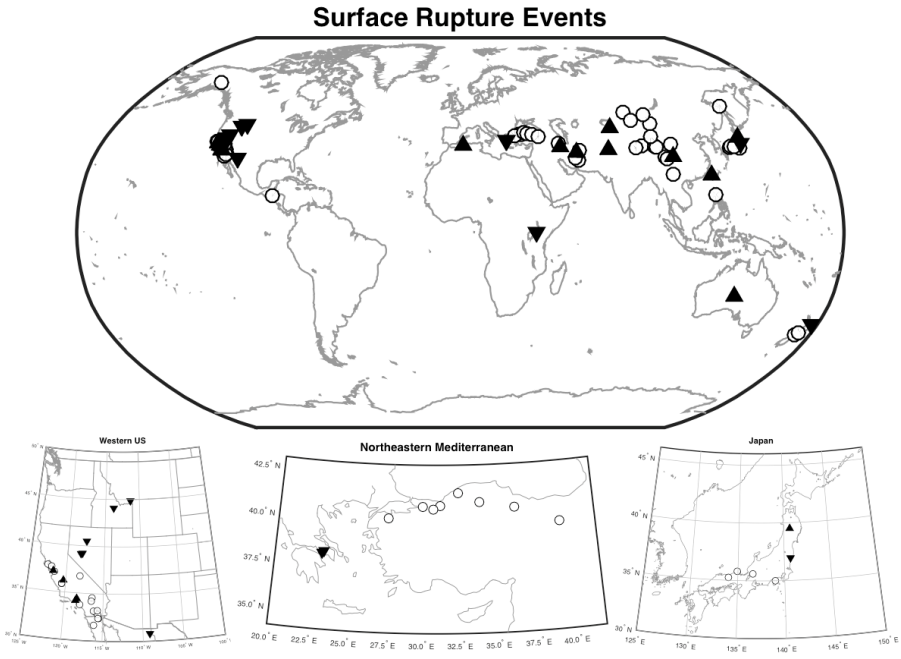

Figure 3: Locations of events considered in this study. Open circles show locations of events with a strike-slip mechanism. Upward-pointed triangles represent reverse events, and downward-pointed triangles represent normal mechanisms.

4 Modeling Approaches

We fit the data with three models, each of which is described in greater detail described in the Appendix. The first, M1, explores a linear regression of Mw with the logs of length and slip rate:

$$M_W = c_0 + c_1 \log L_E + c_2 \log \frac{S_F}{S_0} \tag{1}$$

where L_E is the rupture length measured along strike, S_F is the long-term average geological slip rate on the fault, M_W is moment magnitude (Kanamori, 1977), and c_0, c_1, and c_2 are three unknown coefficients. Mathematically, c_0 trades off with $c_2 \log S_0$, so the parameter S_0 is set equal to the log average slip rate for the ensemble of events with the considered focal mechanisms. Based on equations in the Appendix, the stress drop varies continuously with L_E in model M1. With this convention, Equation 1 with $c_2 = 0$ provides the best model when S_F is unknown. Two misfit parameters are considered. The first, σ_1 is the standard deviation of the difference between observed and predicted magnitudes when $c_2 = 0$, while σ_3 is the corresponding standard deviation when the slip rate term in Equation 1 is incorporated.

The second, M2, has constant stress-drop slopes for small and large earthquakes:

$$\begin{aligned} M_W &= M_{bp} + c_{1C}\log(\tfrac{L_E}{L_{bp}}) + c_2\log\left(\tfrac{S_F}{S_0}\right) \quad L_E < L_{bp} \\ M_W &= M_{bp} + c_{1L}\log(\tfrac{L_E}{L_{bp}}) + c_2\log\left(\tfrac{S_F}{S_0}\right) \quad L_E \geq L_{bp} \end{aligned} \tag{2}$$

where $c_{1C} = 2$ and $c_{1L} = 2/3$. As described further in the Appendix, models for the scaling of a small fault with constant stress drop have slope $c_{1C} = 2$, while models for a long fault have slope $c_{1L} = 2/3$ (e.g. Kanamori and Anderson, 1975). Equation 2 does not require the stress drop to be the same for small and large earthquakes. The three unknown parameters in model M2 are L_{bp}, the rupture length where the slope changes from 2 to 2/3, M_{bp}, the magnitude at that transition, and c_2 which is again the sensitivity of magnitude to fault slip rate. Thus Equation 2 has the same number of unknown parameters to be determined from the data as Equation 1.

In the third model, M3, maintains a constant stress drop, $\Delta\tau_C$, for all rupture lengths according to the relationships of Chinnery (1964):

$$M_W = \begin{cases} 2\log L_E + \frac{2}{3}\log\Delta\tau_C + \frac{2}{3}\left(\log\frac{2\pi}{C_{LW}C(\gamma)} - 16.1\right) + c_2\log\left(\frac{S_F}{S_0}\right) & \frac{L_E}{C_{LW}} < W_{max} \\ \frac{2}{3}\log L_E + \frac{2}{3}\log\Delta\tau_C + \frac{2}{3}\left(\log\frac{2\pi W_{max}^2}{C(\gamma)} - 16.1\right) + c_2\log\left(\frac{S_F}{S_0}\right) & \frac{L_E}{C_{LW}} \geq W_{max} \end{cases} \tag{3}$$

where

$$C(\gamma) = 2\cos\gamma + 3\tan\gamma - \frac{\cos\gamma\sin\gamma\,(3 + 4\sin\gamma)}{(1+\sin\gamma)^2} \tag{4}$$

and γ is the angle from the top center of the fault to either of the bottom corners, i.e. $\tan\gamma = 2W_E/L_E$. The Appendix describes the Chinnery (1964) model, and its adaptation to obtain Equation 3. This model depends on four parameters. These are the aspect ratio of the fault for small ruptures, $C_{LW} = L_E/W_E$, the maximum fault width W_{max} at which, if the selected aspect ratio implies a width greater than W_{max} the width is set to W_{max}, the stress drop, $\Delta\tau_C$, and c_2, the coefficient that quantifies the slip rate dependence.

Model Equations 1, 2, and 3 require different strategies to obtain their unknown coefficients. The simplest way to find the unknown coefficients for Equation 1 is by using a linear least-squares regression, which minimizes the misfit of the prediction of M_W, but does not account for uncertainties in L_E or S_F. ASW96 approached this difficulty by carrying out multiple regressions for points chosen at random within the range of allowed values of all three parameters, and then looked at the distribution of derived values of the inferred constants. Alternative approaches to find the coefficients, described variously as "total least squares" or "general orthogonal regression" (e.g. Castellaro et al., 2006; Castellaro and Borman, 2007; Wikipedia article "Total Least Squares" accessed Feb. 15, 2015) were also considered. The approach by ASW96 turned out to give the least biased results for a set of synthetic data with an uncertainty model that we considered to be realistic and consistent with the actual data, so their approach is also used in this study.

Equation 2 has the additional complication of being non-linear in L_{bp}. We approach the solution by reorganizing Equation 2 as

$$M_{bp} + c_2 \log\left(\frac{S_F}{S_0}\right) = M_W - c_{1x} \log\left(\frac{L_E}{L_{bp}}\right) \quad (5)$$

where c_{1x} is either c_{1C} or c_{1L} depending of L_E . Assuming a value for L_{bp}, it is straightforward to find the unknown coefficients M_{bp} and c_2 . We considered a set of closely-spaced values of L_{bp} from the smallest to the longest rupture length in the data, and choose the value with the smallest total misfit. As in the linear case, we solved for the coefficients of Equation 5 multiple times with randomized values of M_W, L_E, and S_F, and our preferred model is the mean of the coefficients from the multiple realizations.

Model M3 (Equation 3) has four unknown parameters, where the effects of C_{LW} and W_{max} are nonlinear (Appendix, Figure 18). For this reason, a grid search was performed. For each of 506 combinations on a grid of C_{LW} and W_{max}, 10,000 realizations of fault parameters were fit with optimal values of $\Delta\tau_C$ and c_2. The combinations that optimized magnitude misfit neglecting the slip rate (σ_1) and including the slip rate (σ_3) were identified. The minima in σ_1 and σ_3 did not generally occur for the same combinations of C_{LW} and W_{max}, so some judgement was involved in the parameter selection. Because the results of model M3 might potentially be used for faults where slip rate is unknown, we favored minimizing σ_1, but as the minimum in σ_1 was broad, it was possible to select C_{LW} and W_{max} to nearly minimize σ_1 where σ_3 was also small. The grid limits were chosen to only include maximum fault widths that were considered reasonable from a physical standpoint, while also noting the suggestions of Shaw and Scholz (2001), King and Wesnousky (2007), and Shaw and Wesnousky (2008) that a dynamic rupture in a large earthquake might reasonably extend deeper than the brittle crustal depths associated with microearthquakes.

5 Analysis Results

Figures 4, 5, and 6 show results for strike-slip data sets for the three models. Next, Figures 7, 8, and 9 show equivalent results for the set of reverse faults. Figures 10, 11, and 12 show equivalent results for the normal faults. Finally, for continuity with ASW96, Figures 13, 14, and 15 show the results for combined data sets, but as will be discussed subsequently the value of this combined model is subject to challenge and we do not recommend its use. Model coefficients for models M1, M3, and M3 are given in Tables 3, 4, and 5, respectively. For each model, the coefficients and their uncertainties in Tables 3, 4, and 5 are based on 10,000 regressions where, for each, M_W, L_E, and S_F are chosen at random from the range of uncertainties given in the Online Supplement. The standard deviations of M_W from the models without considering slip rate, σ_1, and including the effect of the slip rate, σ_3, are the average values from the

10,000 realizations. These are also given in Tables 3, 4, and 5, and shown on the figures.

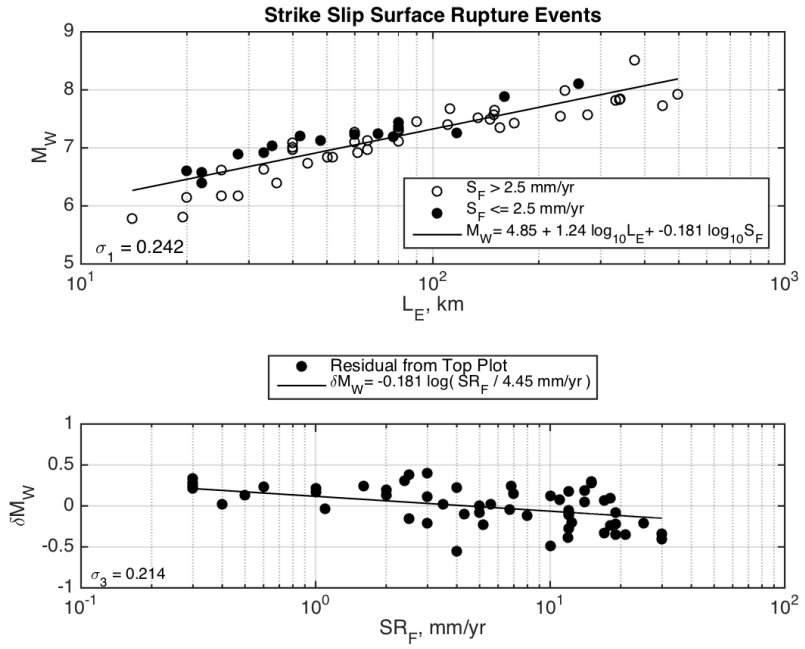

Figure 4: The linear model, M1, applied to the strike-slip earthquakes in Tables 1 and 2. *Upper frame* shows M_W plotted as aa function of L_E. Points are all the preferred values, as given in the Tables. Solid points represent low slip-rate faults. The solid line uses coefficients given in Table 3 and the average value of S_F, 4.45 mm/yr in this case. The lower frame shows the residuals of the points in the upper frame from the shown linear model. The solid line shows the predicted effect of S_F based on the coefficients in Table 3. The significant effect of fault slip rate is seen in the clear separation of low and high slip-rate faults in the upper panel, and the significant slope in the lower panel.

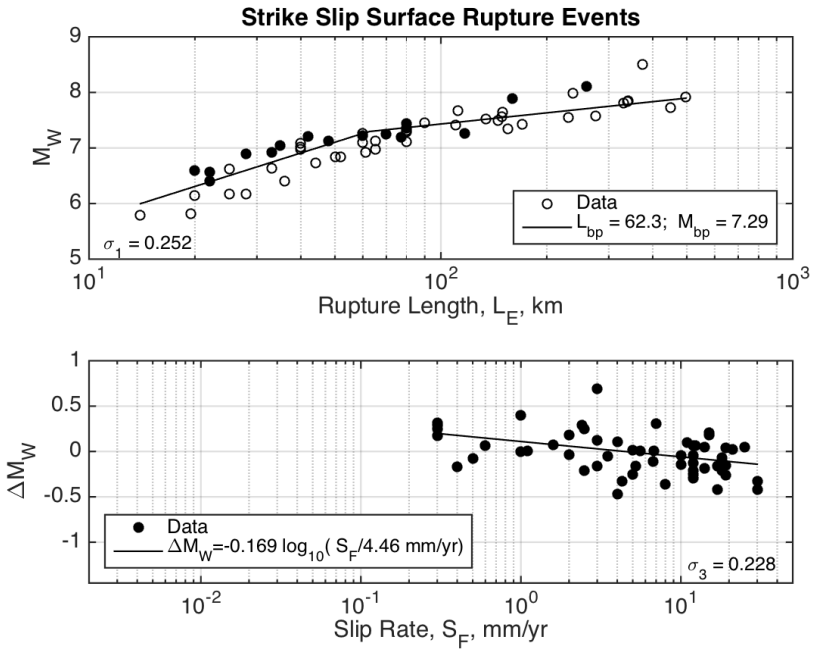

Figure 5: The bi-linear model, M2, applied to the strike-slip earthquakes in Tables 1 and 2. Other figure details are as in Figure 4. Coefficients for the lines are given in Table 4.

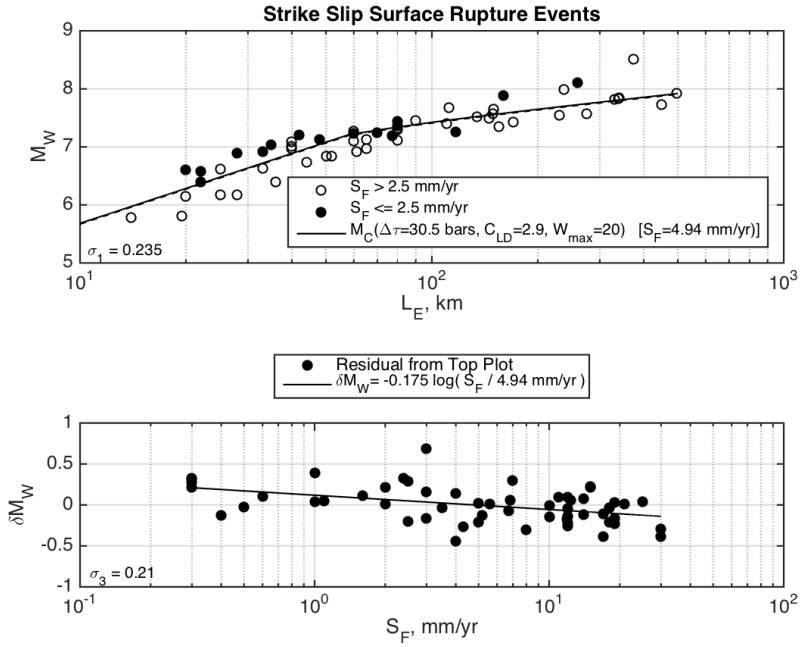

Figure 6: Model M3, applied to the strike-slip earthquakes in Tables 1 and 2. Other figure details are as in Figure 4. Coefficients for the lines are given in Table 5.

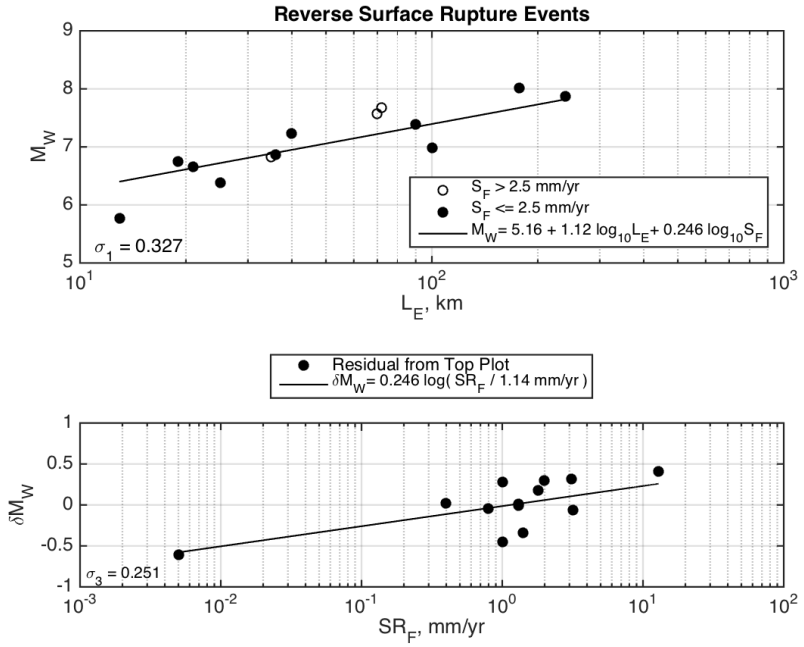

Figure 7: Linear model, M1, is applied to the reverse earthquakes in Tables 1 and 2. Other figure details are as in Figure 4. Coefficients for the lines are given in Table 3.

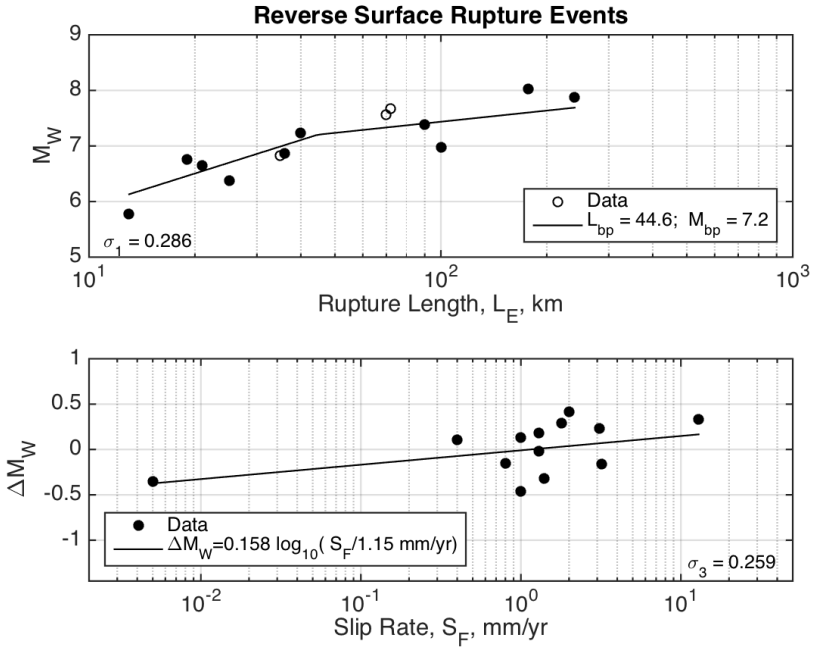

Figure 8: Bi-linear model, M2, applied to reverse earthquakes in Tables 1 and 2. Other figure details are as in Figure 4. Coefficients for the lines are given in Table 4.

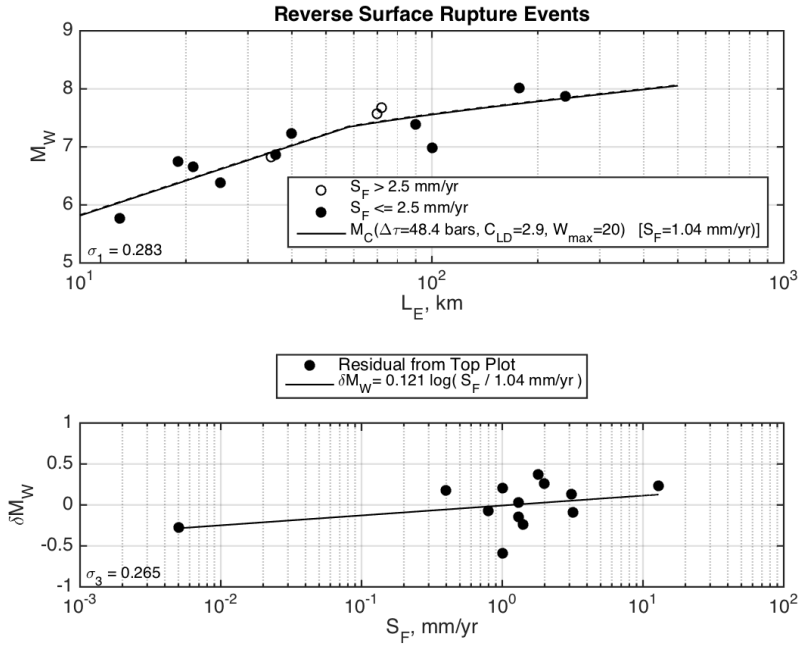

Figure 9: Model M3, applied to the reverse earthquakes in Tables 1 and 2. Other figure details are as in Figure 4. Coefficients for the lines are given in Table 5.

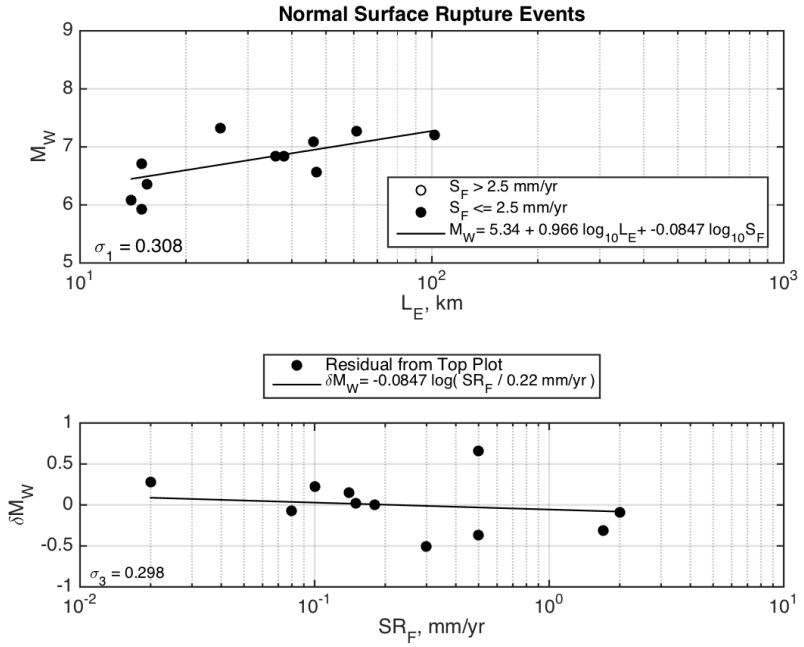

Figure 10: Linear model, M1, applied to the normal earthquakes in Tables 1 and 2. Other figure details are as in Figure 4. Coefficients for the lines are given in Table 3.

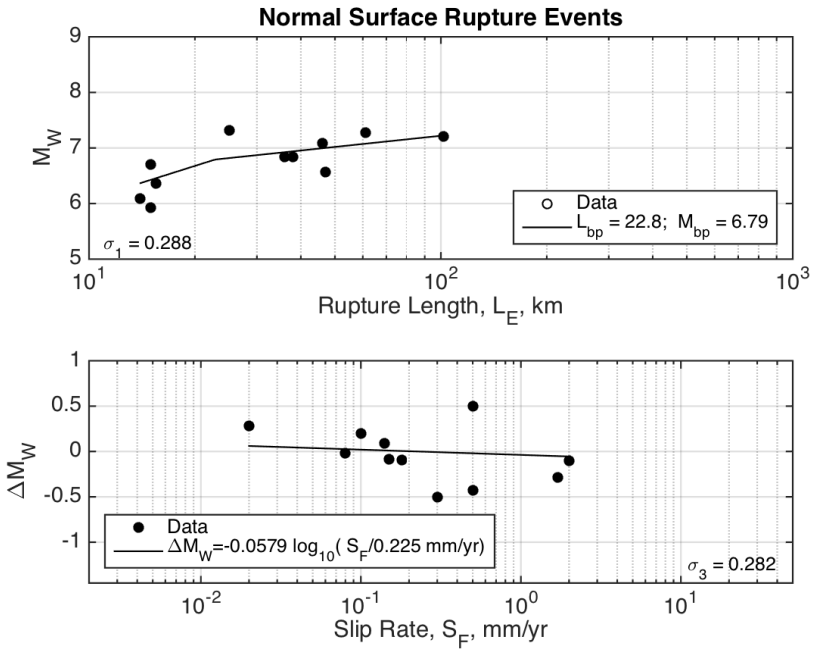

Figure 11: Bi-linear model, M2, applied to the normal earthquakes in Tables 1 and 2. Other figure details are as in Figure 4. Coefficients for the lines are given in Table 4.

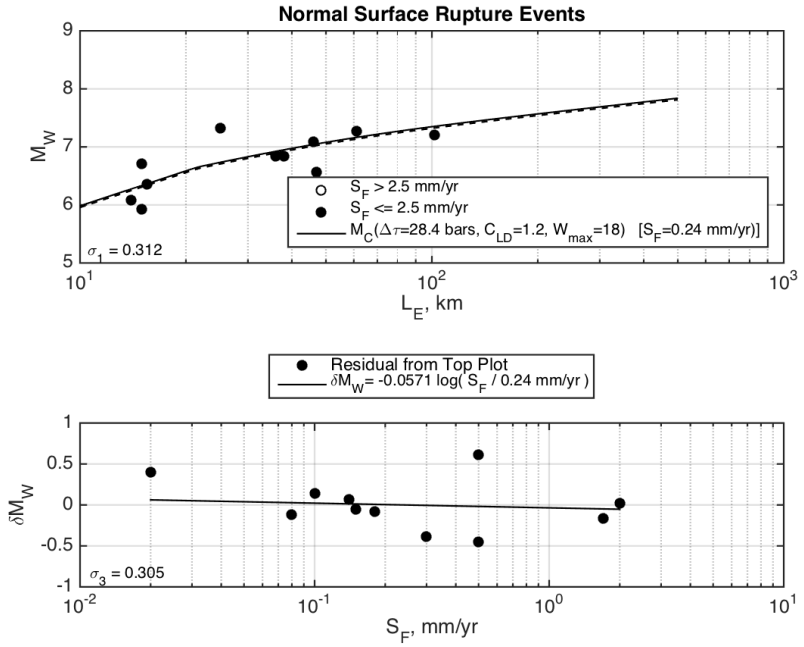

Figure 12: Model M3, applied to the normal earthquakes in Tables 1 and 2. Other figure details are as in Figure 4. Coefficients for the lines are given in Table 5.

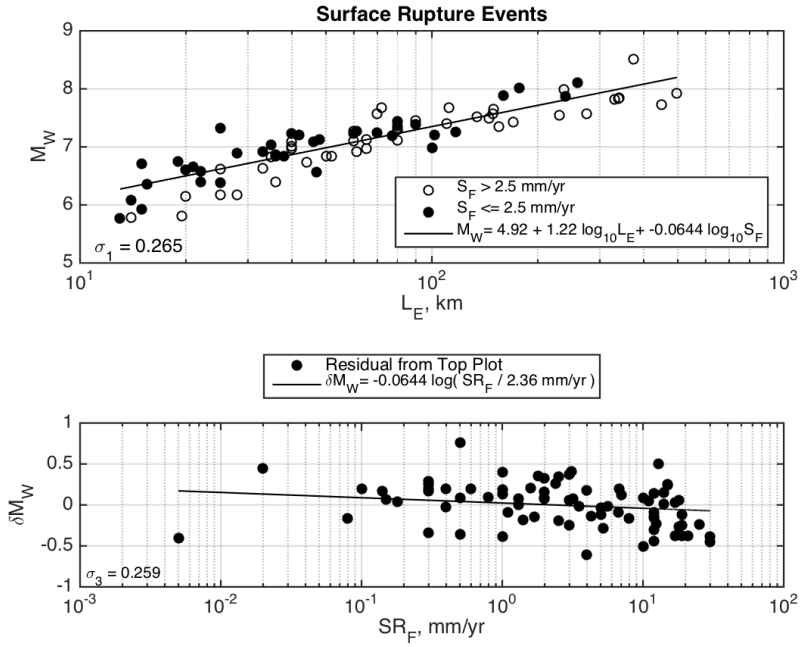

Figure 13: Linear model, M1, applied to all earthquakes in Tables 1 and 2, regardless of mechanism. Other figure details are as in Figure 4. Coefficients for the lines are given in Table 3.

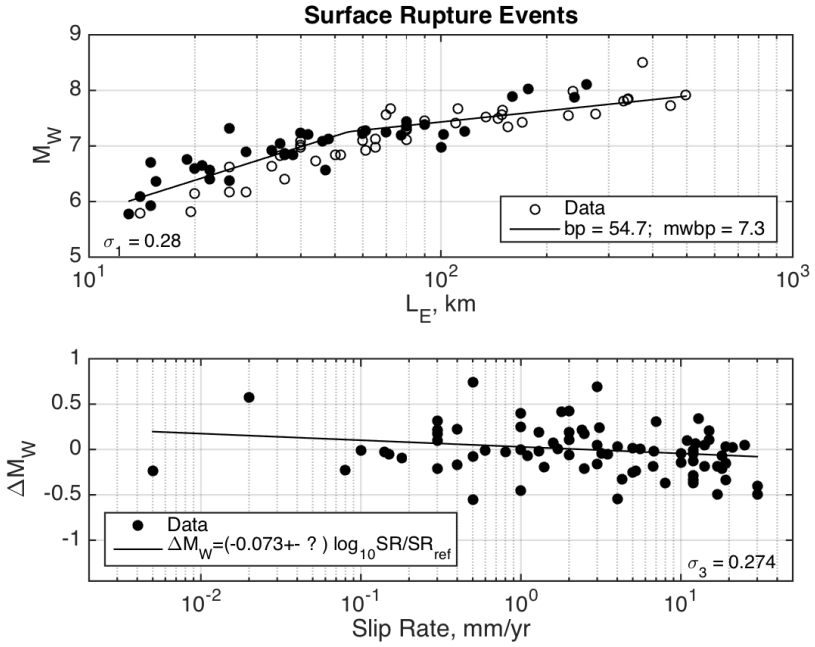

Figure 14: Bi-linear model, M2, applied to all earthquakes in Tables 1 and 2, regardless of mechanism. Other figure details are as in Figure 4. Coefficients for the lines are given in Table 4.

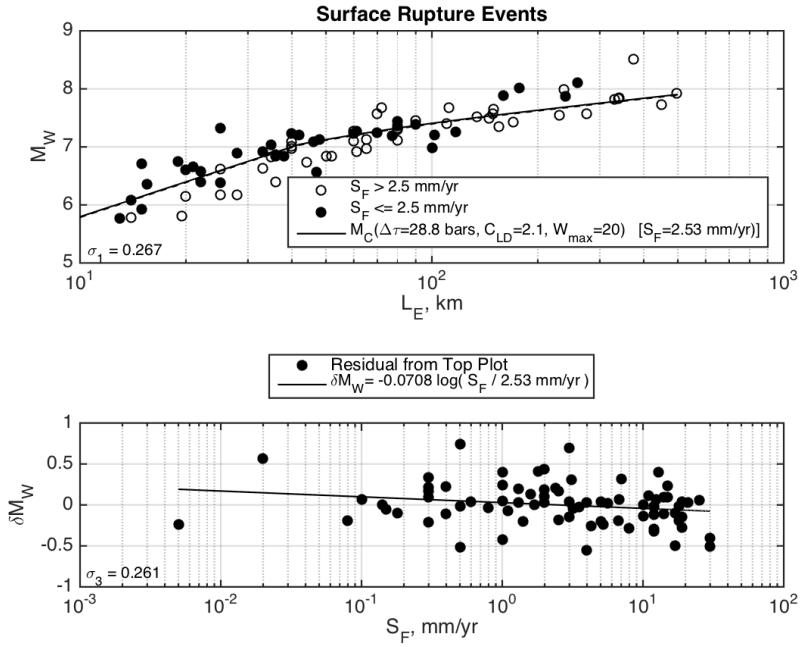

Figure 15: Model M3, applied to all earthquakes in Tables 1 and 2, regardless of mechanism. Other figure details are as in Figure 4. Coefficients for the lines are given in Table 5.

5.1 Linear model

The parameters for the linear models are given in Table 3. As noted previously, the linear model is obtained by solving for the coefficients c_0, c_1, and c_2 of Equation 1 using a standard least-squares regression. Figure 16 shows the distribution of coefficients found for 10,000 trials for strike-slip faults. The widths of these distributions are used to estimate the uncertainty in each coefficient. The coefficients c_0, c_1, and c_2 are found simultaneously, as opposed to a possible alternative approach in which c_0 and c_1 could be found first, and then c_2 determined by a second independent line fit to the residuals.

For strike-slip events, which dominate the data, $c_2 = -0.18$, similar to ASW96 (Figure 4). The data with a reverse mechanism support magnitude increasing, rather than decreasing, with increased slip rate (Figure 7), while for the events with a normal mechanism the slip-rate dependence is not distinguishable from zero (Figure 10). Considering the distribution of slip rate data in Figure 7 , it is apparent that the event with slip rate of 0.005 mm/yr has a very strong influence on the slope of the slip-rate dependence. This is the 1968 Maryat Creek, Australia earthquake, M5.8, #28 in Table 1. As an intracontinental event, one could legitimately question whether it should be included. Relevant

points in this regard are, first that the physics of rupture of crystalline rocks with a crustal composition are not, a-priori, different merely because the fault is located far from a plate boundary. The second point is that the Marryat Creek event tends to decrease the slope of the slip rate dependence, as a consideration of the remaining points will reveal. Nonetheless, if this point were excluded, the domain of the remaining slip rates would be reduced so much that the slope of the line, while positive, would not be distinguishable from zero.

Thus, the results for the linear model challenge the validity of models that combine the different faulting types. The ASW96 model was $M_W = 5.12 + 1.16 \log L_E - 0.20 \log S_F$, which is only slightly different from Figure 13, and the uncertainty for the combined data set is 0.259, which is not distinguishable to the value of 0.26 in ASW96. This result demonstrates continuity with the previous study. However, the results separated by mechanism indicate that this trend is dominated by strike slip, while the normal mechanisms show little or no slip-rate dependence, and the reverse mechanisms potentially showing a different dependence. Suppose as a thought experiment that the dip-slip cases are pure noise. A strong strike-slip case plus some noise will still resolve to a decently significant trend even though we added only noise. The problem in the combined regression becomes we would use it to project back from the strong case into the noise, and say things about future dip-slip earthquake expectations that aren't likely based on the available data.

Table 3: Parameters for the linear model, M1, given by Equation 1, for the different fault types considered separately, and for the combined set of all earthquakes listed in Table 1 and 2.

	Strike-Slip	Reverse	Normal	Combined
c_1	4.85±0.0588	5.16 ± 0.095	5.34 ± 0.175	4.92 ± 0.0481
c_2	1.24 ± 0.0292	1.12 ± 0.0562	0.966 ± 0.118	1.22 ± 0.025
c_3	-0.181 ± 0.0198	0.246 ± 0.0326	-0.0874 ± 0.0863	-0.0644 ± 0.0131
S_0	4.45 mm/yr	1.14 mm/yr	0.22 mm/yr	2.36 mm/yr
σ_1	0.242	0.327	0.308	0.265
σ_3	0.214	0.251	0.298	0.259

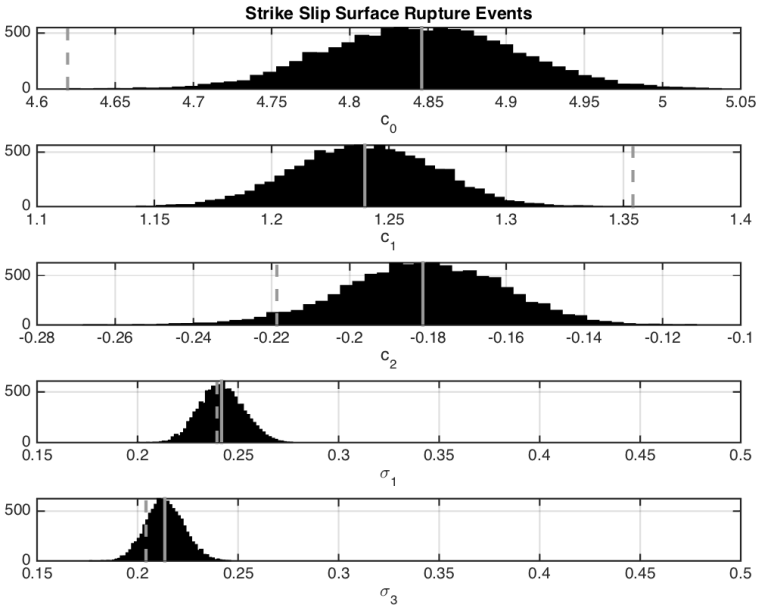

Figure 16: Coefficient distribution, linear, strike-slip case. The bar chart shows number of occurrences of parameter values among 10,000 realizations for randomly selected values of Mw, LE, and SF within the uncertainty range of each. Solid gray line shows the mean value of each parameter. The dashed grey line shows the value found for the preferred value of Mw, LE, and SF for each earthquake. The clear negative value of c2 corresponds to decreasing relative magnitude predictions with increasing slip rate.

5.2 Bilinear, with optimum break point

The bilinear model is calculated following the approach described in Equation 5. Figure 17 shows an example of the distribution of coefficients for the reverse mechanism case. Table 4 gives coefficients for the bilinear models. The results are mixed, with some cases showing small but generally not statistically significant increase in σ_1 and σ_3 compared to the linear case.

For the strike-slip case, the fit to the data in Figure 5 is better at large rupture lengths than in Figure 4. At large lengths, the point in Figures 4 and 5 plotted at 375 km and M8.5 is the 1905 Mongolia, earthquake. There is uncertainty in how to measure the rupture length, as the 375 km length does not include a spur fault that is 100 km long; at 475 km total rupture length, this event would be less of an outlier. For this and other reasons, the Bulnay, Mongolia event is recognized as exceptional. This and other complexities in how to measure rupture length need future study.

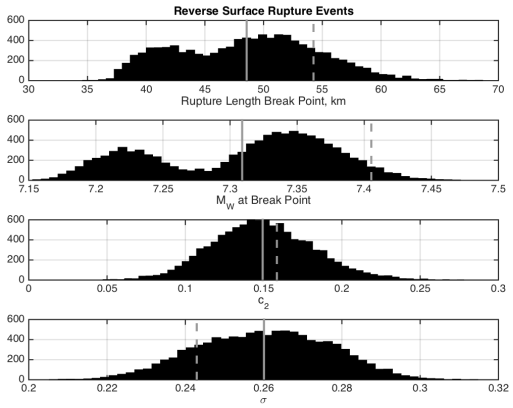

Figure 17: Bilinear - coefficients for reverse faulting. Other figure details are as in Figure 16.

Table 4: Bilinear model coefficients

	Strike-Slip	Reverse	Normal	Combined
L_{bp}	62.2± 5.49	44.6± 5.07	22.8 ± 1.66	54.7 ± 3.23
M_{bp}	7.29± 0.0432	7.20± 0.0686	6.79± 0.0359	7.26± 0.0295
c_2	-0.170± 0.0272	0.158± 0.0323	-0.0596± 0.0714	-0.0726± 0.0151
S_0	4.46	1.15	0.225	2.36
σ_1	0.252	0.286	0.288	.280
σ_3	0.228	0.259	0.282	.274

5.3 Constant stress drop model

Parameters for the constant stress drop model M3 are given in Table 5. For strike-slip cases, this approach has smaller values of both σ_1 and σ_3 than either models M1 or M2. While this improvement is small, it is encouraging that a model with constant stress drop achieves this result. W_{max} for this model is in the range suggested by King and Wesnousky (2007). The optimal aspect ratio of 2.9 is smaller than suggested by Shaw and Scholz (2001). For the reverse faulting data we considered values of L_{max} up to 30 km since reverse faults can have low dips, and that upper limit is the preferred value. M3 has a smaller value of σ_1 than M1 or M2 for the reverse faulting case, but the slip rate was not as effective at decreasing σ_3 in M3 as in M1. For normal faulting, M1 has a slight edge over M3.

Table 5: Chinnery model coefficients

	Strike-Slip	Reverse	Normal	Combined
$\Delta\tau_C$, bars	30.5	48.4	28.4	28.8
C_{LW}	2.9	1.4	1.2	2.1
L_{max}, km	20	30	18	20
c_2	-0.175	0.121	0.057	-0.071
S_0, mm/yr	4.94	1.04	0.24	2.53
σ_1	0.235	0.283	0.312	0.267
σ_3	0.210	0.265	0.305	0.261

6 Discussion

The larger data set modeled here compared to ASW96 expands our understanding of slip rate dependence. Statistically significant improvements are realized with slip rate dependence for strike-slip faults for all three models considered here. On the other hand, individual models for reverse and normal faulting have, at best, an equivocal place for slip rate dependence. For linear and bilinear models of the normal faulting events, but not the constant stress drop model, at least the sign of slip rate dependence agrees with strike-slip. Thus normal faulting could could have slip rate dependence toward smaller magnitudes for higher slip rate faults, but just lack sufficient data to prove it. The reverse faulting events disagree even at the sign of the effect. The disagreement is present whether we retain either or both of the apparent outliers in Figures 7-9. Thus based on the current data, we do not find support for the general reduction of magnitude with slip rate implied by the combined set regression. It appears that the strength of the slip rate effect among strike slip events and their shear numbers relative to dip slip events overwhelm the ambiguous (normal) and contrary (reverse) data, leading to an apparently general slip-rate relationship among all data. Thus our new data set contributes the understanding that slip rate dependence is dominantly a strike-slip fault effect that is not inconsistent with normal faulting, and not apparently consistent with reverse mechanism fault rupture. The data available to ASW96 did not permit this distinction.

If we are guided by studies of earthquake source physics, model M3 may be preferable to M1 or M2. Specifically, the advantage would be the apparently constant stress drop of earthquakes over the full range of magnitudes, consistent with e.g. Allmann and Shearer (2009). The slope of the linear model, M1, with rupture length implies that stress drop increases significantly with rupture length. The slopes of the bilinear model, M2, are consistent with simple models for scaling with constant stress drop in the small and large earthquake domains, but the stress drops in the two domains are different. In addition, since the buried circular rupture model by construction does not reach the surface, its applicability to the short ruptures of M2 is not obvious.

Constant stress drop model M3 has the important advantage compared to dislocation models in a half-space, in that it is explicitly designed for surface-

rupturing earthquakes. Stress differences due to the free surface effect of rupture are recognized as having significant effects on ground motion. For this reason we can expect that it will perform well where magnitude scaling is required for application to strong ground motions. In exchange the Chinnery (1964) model has a singularity of stress drop near its edges, which enables a closed form solution. This approximation is probably no more significant than those already made to summarize spatial variability in recordings of actual individual earthquakes. The application of the same functional form for dip-slip earthquakes is entirely ad-hoc, of course. Although it is more complicated, its consistency with a physical model with a constant stress drop commends it as a preferred regression. Compared with the better-known equations summarized by Kanamori and Anderson (1975), the stress drop parameter in this model is smaller, emphasizing that all stress drop estimates are model dependent.

The decreased magnitude for high-slip rate strike-slip faults implies that the stress drop on those faults is lower. The finding is consistent with the hypothesis of Kanamori and Allen (1986) that a longer healing time results in a larger stress required to initiate rupture, and thus a higher stress drop. For normal or reverse faulting, the slip-rate dependence is low, and the slip-rate coefficient c2 is indistinguishable from zero. The findings suggest that, if c2 is not zero for these cases, then c2 is positive for reverse faulting earthquakes. This is contrary to the hypothesis of Kanamori and Allen. We suggest that if this positive slope is confirmed with added data, the physical mechanism may be related to the dynamics of rupture. For a reverse fault, the dynamic stresses on a rupture propagating updip are tensile as rupture approaches the surface, so the coefficient of friction or cohesion on the fault is less relevant.

There are a number of future studies that should be performed to improve upon the results presented here. The first is to examine the consistency of the models, and especially M3, with observed fault displacement. If the results, based on the definition of seismic moment (Equation 7) agree with seismic data, the scaling relationship presented here would be an alternative to the self-consistent scaling model of Leonard (2010, 2014) for earthquakes in continental crust.

A second issue that deserves study is to consider if there is an optimal way to handle multi-segment faults in the data considered here. The study needs to consider how seismic moment is distributed on multiple segments, as well as how best to measure the lengths of multiple segment ruptures. The problem with the Bulnay, Mongolia, earthquake was mentioned above as an example of the uncertainty associated with this issue. Several other faults in Table 1 and 2 have similar issues. If the result is different from the approach used by UCERF3, it could have a direct impact on future seismic hazard analyses.

7 Conclusions

The primary question asked by this research is if the introduction of slip rate on a fault helps to reduce the uncertainties in estimates of magnitude from

observations of rupture length. We find that such a slip rate dependence is well established for strike-slip cases: as the slip rate increases, the predicted magnitude tends to decrease. This result is robust in the sense that it is present and statistically significant for all three of the considered models relating rupture length and magntiude. For reverse and normal faulting mechanisms, on the other hand, our data do not demonstrate the presence of a significant slip rate effect in the relationship between rupture length and magnitude.

The constant stress drop model presented here has potential for progress on a standing difficulty in ground motion modeling of an internally consistent scaling of magnitude, length, down-dip width, and fault displacement. Current relations in which magnitude scales with length or area lead to unphysical stress drops or unobserved down-dip widths, respectively. Constant stress drop alternatives such as Shaw (2009) require complex scaling arguments and difficult to constrain parameters. By working from the model of Chinnery (1964) our constant stress drop model has the advantage of starting with realistic physics including the stress effects of surface rupture. Work remains in validating displacements from our model, but the fact that it fits the current magnitude-length-slip rate data as well or a bit better than the linear and bilinear models suggests that the Chinnery-based constant stress drop has promise for modeling earthquake effects.

8 Resources

The Wikipedia article "Total Least Squares" was accessed Feb. 15, 2015.

9 Acknowledgements

Research supported by the U.S. Geological Survey (USGS), Department of the Interior, under USGS award number G14AP00030. The views and conclusions contained in this document are those of the authors and should not be interpreted as necessarily representing the official policies, either expressed or implied, of the U.S. Government.

10 References

Abercrombie, R. (1995). Earthquake source scaling relationships from -1 to 5 M_L using seismograms recorded at 2.5-km depth, J. Geophys. Res. 100, 24,015-24,036.

Allmann, B. P. and P. M. Shearer (2009). Global variations of stress drop for moderate to large earthquakes, J. Geophys. Res. 114, B01310, doi:10.1029/2008JB005821.

Anderson, J. G. (1986). Implication of attenuation for studies of the earthquake source, Earthquake Source Mechanics, Geophysical Monograph 37, (Maurice Ewing Series 6), American Geophysical Union, Washington, D.C. 311-318.

Anderson, J. G., S. G. Wesnousky and M. Stirling (1996). Earthquake size as a function of fault slip rate, Bull. Seism. Soc. Am. 86, 683-690.

Anderson, J. G., J. N. Brune, M. Purvance and A. Anooshehpoor (2005). Data needs for improved probabilistic seismic hazard analysis, in Directions in Strong Motion Instrumentation, Edited by Polat Gulkan and John G. Anderson, NATO Science Series, IV. Earth and Environmental Sciences – Vol. 58, Springer, Dordrecht, The Netherlands, 1-24.

Baltay, A., G. Prieto and G. C. Beroza (2010). Radiated seismic energy from coda measurements and no scaling in apparent stress with seismic moment, J. Geophys. Res., 115, B08314, doi:10.1029/2009JB006736.

Baltay, A., S. Ide, G. Prieto and G. Beroza (2011). Variability in earthquake stress drop and apparent stress, Geopyhys. Res. Lett., 38, L06303, doi:10.1029/2011GL046698.

Bormann, P., S. Wendt and D. DiGiacomo (2012). CHAPTER 3: Seismic Sources and Source Parameters DOI:10.2312/GFZ.NMSOP-2_CH3, in Bormann, P. (Ed.) (2012). New Manual of Seismological Observatory Practice (NMSOP-2), IASPEI, GFZ German Research Centre for Geosciences, Potsdam; http://nmsop.gfz-potsdam.de; DOI: 10.2312/GFZ.NMSOP-2, urn:nbn:de:kobv:b103-NMSOP-2.

Castellaro,S., F. Mulargia and Y. Y. Kagan (2006). Regression problems for magnitudes, Geophys. J. Int. (2006) 165, 913–930 doi: 10.1111/j.1365-246X.2006.02955.x

Castellaro, S. and P. Bormann (2007). Performance of Different Regression Procedures on the Magnitude Conversion Problem, Bulletin of the Seismological Society of America, Vol. 97, No. 4, pp. 1167–1175, August 2007, doi: 10.1785/0120060102.

Chinnery, M. A. (1963). The stress changes that accompany strike-slip faulting, Bulletin of the Seismological Society of America. Vol. 53, No. 5, pp. 921-932.

Chinnery, M. A. (1964). The Strength of the Earth's Crust under Horizontal Shear Stress, J. Geophys. Res. 59, 2085-2089.

Dieterich, J. H. (1972). Time dependent friction in rocks, J. Geophys. Res. 20, 3690-3704.

Hanks, T. C., and W. H. Bakun (2002). A bilinear source-scaling model for Mlog A observations of continental earthquakes, Bull. Seismol. Soc. Am. 92, no. 5, 1841–1846.

Hanks, T. C., and W. H. Bakun (2008). Mlog A observations for recent large earthquakes, Bull. Seismol. Soc. Am. 98, no. 1, 490–494.

Hanks, T. C. and H. Kanamori (1979). A moment magnitude scale, J. Geophys. Res. 84, 2348-2350.

IASPEI (2005). Summary of Magnitude Working Group recommendations on standard procedures for determining earthquake magnitudes from digital data. http://www.iaspei.org/commissions/CSOI/summary_of_WG_recommendations_2005.pdf

IASPEI (2013). Summary of Magnitude Working Group recommendations on standard procedures for determining earthquake magnitudes from digital

data. http://www.iaspei.org/commissions/CSOI/Summary_WG_recommendations_20130327.pdf

Ide, S., G. C. Beroza, S. G. Prejean and W. L. Ellsworth (2003). Apparent break in earthquake scaling due to path and site effects on deep borehole recordings, J. Geophys. Res. 108, 2271, doi:10.1029/2001JB001617.

Iida, K. (1959). Earthquake energy and earthquake fault, Nagoya University, J. Earth Sci. 7, 98-107.

Kanamori, H. (1977). The energy release in great earthquakes, J. Geophys. Res. 82, 2981-2987.

Kanamori, H. and C. R. Allen (1986). Earthquake repeat time and average stress drop, Earthquake Source Mechanics S. Das, J. Boatwright, and C. H. Scholz (Editors), Geophysical Monograph 37, 227-235.

Kanamori, H., and D. L. Anderson (1975). Theoretical basis of some empirical relations in seismology, Bull. Seismol. Soc. Am 65, no. 5, 1073–1095.

King, G. C. P. and S. G. Wesnousky (2007). Scaling of fault parameters for continental strike-slip earthquakes, Bull. Seism. Soc. Am. 97, 1833-1840.

Leonard, M. (2010). Earthquake fault scaling: Relating rupture length, width, average displacement, and moment release, Bull. Seismol. Soc. Am. 100, no. 5, 1971–1988, doi: 10.1785/0120090189.

Leonard, M. (2012). Erratum: Earthquake fault scaling: relating rupture length, width, average displacement, and moment release, Bull. Seismol. Soc. Am. 102, 2797.

Leonard, M. (2014). Self-Consistent Earthquake Fault-Scaling Relations: Update and Extension to Stable Continental Strike-Slip Faults, Bull. Seism. Soc. Am. 104, 2953–2965, doi: 10.1785/0120140087.

Rolandone, F., R. Bulrgmann, and R. M. Nadeau (2004), The evolution of the seismic-aseismic transition during the earthquake cycle: Constraints from the time-dependent depth distribution of aftershocks, Geophys. Res. Lett., 31, L23610, doi:10.1029/2004GL021379.

Sato, R. (1972). Stress drop for a finite fault, J. Phys. Earth, 20, 397-407.

Scholz, C. H. (1982). Scaling laws for large earthquakes: consequences for physical models, Bull. Seismol. Soc. Am. 72, 1–14.

Scholz, C. H., C. A. Aviles, and S. G. Wesnousky (1986). Scaling differences between large intraplate and interplate earthquakes, Bull. Seism. Soc. Am. 76, 65-70.

Shaw, B. E. (2009). Constant stress drop from small to great earthquakes in magnitude-area scaling, Bull. Seismol. Soc. Am. 99, no. 2A, 871–875.

Shaw, B. E., and C. H. Scholz (2001). Slip-length scaling in large earthquakes: Observations and theory and implications for earthquake physics, Geophys. Res. Lett. 28, no. 15, 2995–2998.

Shaw, B. E., and S. G.Wesnousky (2008). Slip-length scaling in large earthquakes: The role of deep-penetrating slip below the seismogenic layer, Bull. Seismol. Soc. Am. 98, 1633–1641.

Scholz, C. (1982). Scaling laws for large earthquakes: Consequences for physical models, Bull. Seismol. Soc. Am. 72, no. 1, 1–146.

Tocher, D. (1958). Earthquake energy and ground breakage, Bull. Seism. Soc. Am. 48, 147-153.

Wells, D. L., and K. J. Coppersmith (1994). New empirical relationships among magnitude, rupture length, rupture width, rupture area, and surface displacement, Bull. Seismol. Soc. Am. 84, no. 4, 974–1002.

11 Appendix 1: Fault scaling relations

11.1 Basics

This paper proposes models to estimate the moment magnitude of earthquakes based on observed surface rupture lengths. The moment magnitude definition that we use is, implicit in Kanamori (1977):

$$M_W = \frac{2}{3}(\log M_0 - 16.1) \tag{6}$$

The units of seismic moment, M_0, are dyne-cm in Equation 6 . This definition differs slightly from the equation used by Hanks and Kanamori (1979), but is the equation recommended for seismic network operations by the International Association of Seismology and Physics of the Earths Interior (IASPEI, 2005, 2013; Borman et al, 2012), and thus is the relationship used by most seismic networks throughout the world. The seismic moment is defined as:

$$M_0 = \mu A_E \bar{D}_E = \mu L_E W_E \bar{D}_E \tag{7}$$

where μ is the shear modulus, A_E is the fault area ruptured in the earthquake, and $\bar{D}_E$ is the average slip over that area. For a fault that is approximately rectangular, $A_E = L_E W_E$ where L_E is the rupture length measured along strike, and W_E is the downdip rupture width.

Substituting Equation 7 into Equation 6, one obtains (for cgs units)

$$M_W = \frac{2}{3}\log L_E + \frac{2}{3}\log W_E + \frac{2}{3}\log \bar{D}_E + \frac{2}{3}(\log \mu - 16.1) \tag{8}$$

This justifies models that relate magnitude to the log of fault length, width, and mean slip. Slopes different from 2/3 result from correlations between the parameters. Wells and Coppersmith (1996) found that the model

$$M_W = c_1 \log L_E + c_0 \tag{9}$$

predicts magnitude from rupture length with a standard deviation of the misfit, $\sigma_1 = 0.28$.

The possible dependence of stress drop or magnitude on slip rate was recognized by Kanamori and Allen (1986) and Scholz et al. (1986). Equation 9 with the addition of the slip rate term, used by ASW96, is:

$$M_W = c_0 + c_1 \log L_E + c_2 \log S_F \tag{10}$$

Testing for a logarithmic dependence on the geological fault slip rate, S_F, can be motivated by findings in Dieterich (1972). In this paper, we refer to Equation 10 as Model 1, or more briefly M1.

11.2 Constant Stress Drop Scaling

The static stress drop, $\Delta\tau_S$, is the decrease in the shear stress acting on the fault as a result of the earthquake, and is proportional to the ratio of average slip to a fault dimension. Seismic observations have found that the average value of $\Delta\tau_S$ is approximately constant (~4 MPa, ~40 bars) over a broad range of earthquake magnitudes (e.g. Kanamori and Anderson, 1975; Allmann and Shearer, 2009), although there is considerable scatter in these data. Seismic moment, and thus M_W through Equation 6, can be expressed as a function of fault dimension and stress drop, as recognized by Kanamori and Anderson (1975). Selected models are summarized in Table 6.

Table 6: Selected models for the relationship of fault size, stress drop, and M_W.

Case	M_0	Implied magnitude relations[1]
1. Buried, circular[2]	$\frac{16}{7}\Delta\tau_S R_E^3$	$M_W = \log A_E + \frac{2}{3}\log\Delta\tau_S + 3.0089$ (km, bars)
2. Strike-slip, long[2]	$\frac{\pi}{2}\Delta\tau_S W_E^2 L_E$	$M_W = \frac{2}{3}\log L_E + \frac{4}{3}\log W_E + \frac{2}{3}\log\Delta\tau_S + 3.1359$ (km, bars)
3. Dip-slip, long[2]	$\frac{\pi(\lambda+2\mu)}{4(\lambda+\mu)}\Delta\tau_S W_E^2 L_E$	$M_W = \frac{2}{3}\log L_E + \frac{4}{3}\log W_E + \frac{2}{3}\log\Delta\tau_S + 3.3141$ (km, bars)

1. Fault area, $A_E = \pi R_E^2$, in km^2, fault radius R_E, width W_E, and length L_E in km, and stress drop $\Delta\tau_S$ in bars.
2. Cases 1, 2, and 3 are from Kanamori and Anderson (1975).

The equations in Table 6 indicate that constant stress drop implies the slope $c_1 = 2.0$ for small faults (Case 1) and $c_1 = 2/3$ for long faults (Cases 2 and 3). These observations motivate a bilinear approach to fit the data, which is model M2 in the main text of the paper. The bilinear approach is formulated as follows:

$$\begin{aligned} M_W &= M_{bp} + c_{1C}\log(\tfrac{L_E}{L_{bp}}) + c_2\log\left(\tfrac{S_F}{S_0}\right) \quad L_E < L_{bp} \\ M_W &= M_{bp} + c_{1L}\log(\tfrac{L_E}{L_{bp}}) + c_2\log\left(\tfrac{S_F}{S_0}\right) \quad L_E \geq L_{bp} \end{aligned} \tag{11}$$

In Equation 11 the length L_{bp} is the length at which the length-dependence of the scaling relationship changes from the small fault model with slope $c_{1C} = 2$ to the long fault model with slope $c_{1L} = \frac{2}{3}$. The slip rate S_0 is a reference slip rate which can be chosen arbitrarily, but is conveniently chosen to be the log average slip rate in the data, so that setting $S_F = S_0$ gives the best fit when slip rate is unknown. The constant M_{bp} is the magnitude corresponding to a fault with length $L_E = L_{bp}$ and slip rate $S_F = S_0$. Note that Equation 11 has three unknown coefficients (M_{bp}, L_{bp}, and c_2), which is the same number as Equation 10.

However, there are issues with the applicability of the equations 1, 2, and 3 in Table 6. The foremost, for the long faults, is the width of the seismogenic zone. Table 6 shows that W_E is twice as influential as the fault length, so it needs to be considered carefully. One approach to estimate this width is to use the maximum depth of microearthquakes. By this approach, for strike-slip earthquakes the maximum depth of microearthquakes equates directly to an estimate of the fault width, while for a reverse or normal fault the dip is incorporated. The problem is that the maximum depth of seismogenic rupture in large earthquakes is difficult to observe. King and Wesnousky (2007) discuss this difficulty, and present arguments for why the downdip width might be larger in large earthquakes, at least up to some limit than in small earthquakes, because rocks below the depths of mircoearthquakes might experience brittle failure under high strain rates. If the width increases in general for long ruptures, stress drop is no longer as high for these events because stress drop is inversely proportional to W_E, and furthermore the slope c_1 can no longer be reliably constrained by the models in Table 6. King and Wesnousky propose that this explains the proposal by Scholz (1982) that slip in large earthquakes is more nearly proportional to rupture length than to rupture width.

Another issue with the applicability of Equation 1 of Table 6 is that the circular fault model is for an event that is confined within the Earth, while by definition all of the events considered in this study rupture the surface. This motivates development of the model that is described in the next section.

11.3 Relations based on Chinnery (1964)

Chinnery (1963, 1964) calculated a stress drop for a rectangular, strike-slip fault that ruptures the surface. His equations assume a uniform slip on the fault. Thus the stress drop is variable over the fault, and becomes singular at the edge of the fault. His equations give the stress drop on the surface at the midpoint of the rupture. Numerical solutions in Chinnery (1963) show relatively uniform stress drop over large portions of the fault. Chinnery (1963) thus suggests that the results are valid to represent the fault stress drop so long as the zone of slip fall-off is much smaller than the area of the fault. The key advantage provided by this approach is to provide a useful analytical solution.

For the rectangular fault with length L_E, width W_E, and aspect ratio $C_{LW} = L_E/W_E$, the stress drop in the Chinnery model, $\Delta\tau_C$, at the midpoint at the surface is

$$\Delta\tau_C = \frac{\mu \bar{D}_E}{2\pi} C_1 \left(L_h, W_E\right) \tag{12}$$

where

$$C_1 \left(L_h, W_E\right) = \left\{ \frac{2L_h}{aW_E} + \frac{3}{L_h} - \frac{L_h \left(3a + 4W_E\right)}{a \left(a + W_E\right)^2} \right\} \tag{13}$$

Note that $L_h = L_E/2$, and $a = \left(L_h^2 + W_E^2\right)^{\frac{1}{2}}$. Observe that C_1 has dimensions of $1/length$, and thus C_1^{-1} is effectively the fault dimension that is used for

calculating the strain. In other words, the strain change in the earthquake is $\sim \bar{D}_E C_1$. An equation for the seismic moment can be obtained by solving Equation 12 for $\bar{D}_E$ and substituting in Equation 7. The result is

$$M_0 = 2\pi\Delta\tau_C \frac{L_E W_E}{C_1\left(L_h, W_E\right)} \tag{14}$$

and thus

$$M_W = \frac{2}{3}\log L_E + \frac{2}{3}\log\Delta\tau_C + \frac{2}{3}\log\frac{2\pi W_E}{C_1\left(L_h, W_E\right)} - \frac{2}{3}\cdot 16.1 \tag{15}$$

Additional insight into the geometrical term can be obtained by observing that a is the length of the diagonal from the midpoint of the fault at the surface to either of the bottom corners. If the dip of this line is γ, then $\tan\gamma = W_E/L_h = 2/C_{LW}$, $L_h = a\cos\gamma$, $W_E = a\sin\gamma$, and one can rewrite

$$C_1\left(L_h, W_E\right) = \frac{1}{W_E} C\left(\gamma\right) \tag{16}$$

where

$$C\left(\gamma\right) = 2\cos\gamma + 3\tan\gamma - \frac{\cos\gamma\sin\gamma\left(3 + 4\sin\gamma\right)}{\left(1+\sin\gamma\right)^2} \tag{17}$$

Thus one can rewrite Equation 12 as

$$\Delta\tau_C = \frac{C\left(\gamma\right)}{2\pi}\mu\frac{\bar{D}_E}{W_E} \tag{18}$$

Solving Equation 18 for $\bar{D}_E$ and substituting into Equation 7 gives the moment of a vertical strike-slip fault that ruptures the surface as:

$$M_0 = \frac{2\pi}{C\left(\gamma\right)}\Delta\tau_C L_E W_E^2 \tag{19}$$

Because γ, and thus $C\left(\gamma\right)$, depends on the fault aspect ratio, Equations 14, or 19, can be used to model a transition from small-earthquake behavior (e.g. the circular fault in Table 6) to a long-fault behavior. The strategy that is examined in this paper, similar to [refs], is to maintain a constant aspect ratio as the fault length increases, until that aspect ratio implies that the fault width would exceed some maximum. For longer faults, the width is set to that maximum. Before reaching that maximum, γ and $C\left(\gamma\right)$ are constant, and

$$M_0 = \quad \frac{2\pi}{C(\gamma)}\Delta\tau_C\frac{L_E^3}{C_{LW}^2} \quad \frac{L_E}{C_{LW}} < W_{max} \tag{20}$$

For longer faults, for which the width is limited, Equation 19 becomes

$$M_0 = \quad \frac{2\pi}{C(\gamma)}\Delta\tau_C L_E W_{max}^2 \quad \frac{L_E}{C_{LW}} \geq W_{max} \tag{21}$$

In this case, as the fault length increases while width is held constant, γ will be decreasing. For the limit of small γ (roughly $\gamma \lesssim 25^o$) , Equation 17 shows that $C(\gamma) \to 2$, so Equation 14 approaches

$$M_0 = \pi \Delta\tau_C L_E W_{max}^2 \tag{22}$$

Equation 22 differs from Case 2 in Table 6 for the long strike-slip fault by a factor of 2 ($\Delta\tau_S = 2\Delta\tau_C$), where the difference is due to the different boundary conditions used for the two solutions.

From Equations 20 and 21, converting to magnitude, the implied scaling relationship based on the Chinnery model is

$$M_W = \begin{cases} 2\log L_E + \frac{2}{3}\log\Delta\tau_C + \frac{2}{3}\left(\log\frac{2\pi}{C_{LW}C(\gamma)} - 16.1\right) & \frac{L_E}{C_{LW}} < W_{max} \\ \frac{2}{3}\log L_E + \frac{2}{3}\log\Delta\tau_C + \frac{2}{3}\left(\log\frac{2\pi W_{max}^2}{C(\gamma)} - 16.1\right) & \frac{L_E}{C_{LW}} \geq W_{max} \end{cases} \tag{23}$$

Equation 23 will be the third model, M3, considered in this study, with the addition of a slip rate contribution, $+c_2 \log\left(\frac{S_F}{S_0}\right)$, to the two brances of the equation . The unknown parameters in M3 are $\Delta\tau_C$, C_{LW}, W_{max}, and c_2. Thus this model has four parameters to be fit, compared to three parameters in M1 and M2. Figure 18 shows the effect of the three prameters $\Delta\tau_C$, C_{LW}, W_{max} on magnitude predictions. The stress drop scales the entire curve upwards. The aspect ratio C_{LD} adjusts the level of the magnitude for short rupture lengths. The maximum width affects the curvature and how rapidly the curve approaches the asymptotic slope of $\frac{2}{3}\log L_E$ for long rupture lengths.

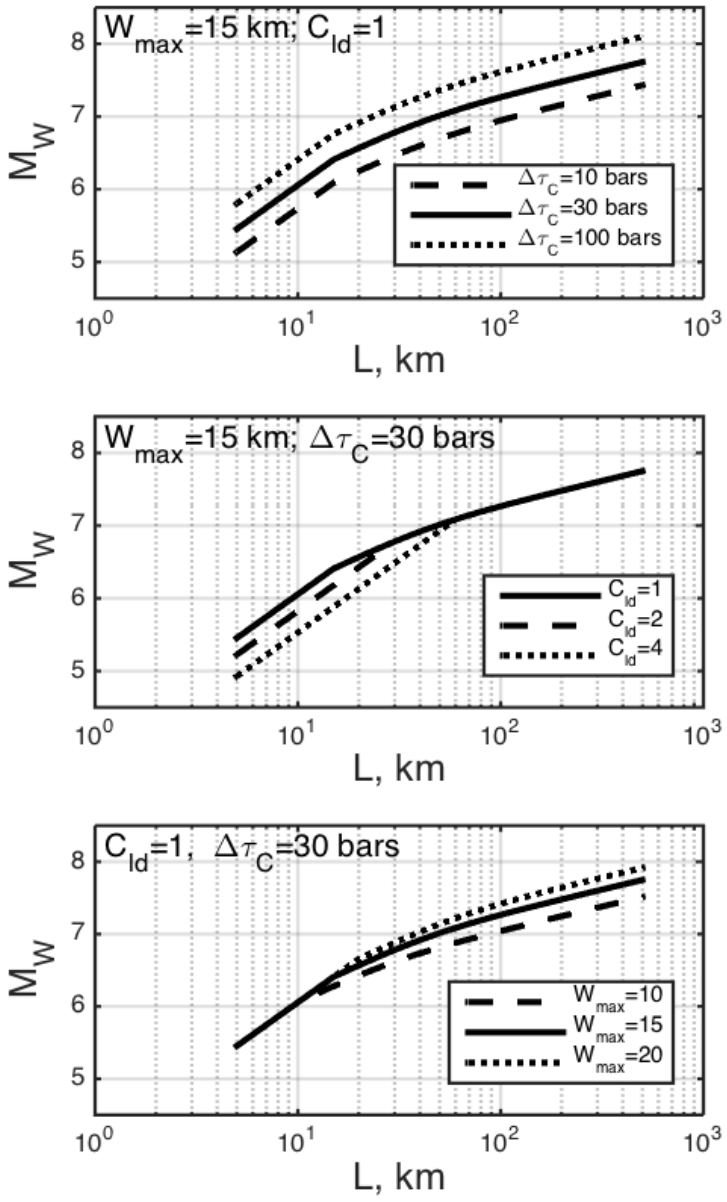

Figure 18: Model for M_W based on Chinnery (1964) scaling as given in Equation 23. Top: effect of changing the stress drop $\Delta\tau_C$. Center: effect of changing the aspect ratio of the fault. Bottom: effect of changing the limiting rupture width W_{max}.

11.4 Other models and considerations

Sato (1972) overcomes the singularity introduced by Chinnery (1963, 1964) by assuming a smooth ad-hoc slip function on a finite, rectangular/elliptical -shaped fault, and for that function, calculated the average stress drop resulting from that slip function. While the results are informative for source physics studies, the major disadvantages of this approach for our application are that the fault is embedded in a whole space, and there is no analytical solution comparable to Equation 12. Rather, the geometrical factor equivalent to $C(\gamma)$ can be computed numerically using equations in Sato (1972) or read from a figure in the paper. Considering these limitations, this model was not considered further.

Shaw and Scholz (2001) and Shaw and Wesnousky (2008) implement a numerical model for fault slip in a half space with depth-dependent friction. They examine the statistics of events that rupture the surface. This paper is interesting for the finding that large surface rupturing events also slip below the brittle crustal depths. The scaling found in the model has properties similar to the scaling in the Chinnery model. However the scaling relationship that they determine has an ad-hoc shape, and thus we preferred the analytical functional form of Chinnery, as discussed above.

Rolandone et al (2004) found some empirical evidence for the penetration of rupture below the brittle seismogenic layer in large earthquakes. They found that the maximum depth of aftershocks of the Landers earthquake were deeper immediately after the main shock, and then the maximum depth returned to pre-earthquake levels over the next few years. This might be explained by high strain rates in the uppermost part of the ductile crust, as high strain rates favor brittle failure. However, post-seismic strain at that depth range would be high even if seismic rupture of the main shock did not extend that deep.

12 Supplemental Online Material

The supplemental material consists of a spreadsheet that includes all earthquakes considered and a list of references for all entries in that spreadsheet.

Spreadsheet: MasterEventTable_2015-10-6.xlsx

References: References_2015_10_06.docx

A conversion of these materials to pdf format is provided here.

66	1	1	0	1/7/1937	Tuosuo Lake - Huashixia	China	SSL	7.6	7.7	7.6	Mw from Mo	3.40E+27	4.30E+27	3.70E+27	Molnar and Deng (1984) not used; length=300 km, overstates Mo. L=150km, Dave=4.1m, from Guo et al. Use 20 km W to get geol Mo: 3.69e+27. min from 10 km variation in length; max=160 km+3.3e11 stiffness M=7.6 & Log Mo = 1.5M + 16.1: 3.16e27	Kunlun Fault	10	12	11	>6.5 ± 1.1 10.8 - 12.4 10 12 - 14 10	Geology Geology Geology Geodesy Geodesy	paleoseismic, Holocene -Alake Late Quaternary and Miocene Holocene Miocene Contemporary Contemporary	Guo et al., 2007; Van Der Woerd et al. (2002), p379 Fu and Awata (2007) Wang et al. (2001) Chen et al. (2000))	145	155	150	Surface Rupture	Guo et al. (2007)	Slip rate in Guo et al., 2007 from paleoseismic trench considered not reliable lower bound.	1	35.404	97.667
67	1	0	0	6/8/1934	Parkfield	California	SSR	6.2	6.4	6.2	Mw from Mo	2.30E+25	4.40E+25	2.30E+25	max: Segall and Du, 1993 (Geodetic); best adopted from Archuleta and Day (1980) from 1966 event and geodetic similarity	San Andreas Fault	21.9	32.6	30	21.9 - 32.6	Geology	late holocene	Toke et al (2011); rate from UCERF3	25	25	25			Assumed to have same rupture length as 1966 event on basis that Segall and Du (1993) obtained identical seismic moment estimates for each.	1	35.88	-120.49
68	1	0	0	3/10/1933	Long Beach	California	SSR	6.4	6.4	6.4	Mw from Mo	5.00E+25	5.00E+25	5.00E+25	Haukksson and Gross (1991)	Newport-Inglewood Fault	1	5	1.1	1 -5	Geology		Treiman and Lundberg (1999); rate from UCERF3	13	25	22	Aftershocks	Haukksson and Gross (1991) (13-16) - (20-25)	Haukksson and Gross (1991) show initial aftershock zone was 13-16 km and extended within hours to 20 - 25 km.	1	33.78	-117.97
69	1	1	0	12/25/1932	Changma	China	SSL, R	7.4	7.7	7.6	Mw from Mo	1.40E+27	5.60E+27	2.80E+27	Molnar and Deng (1984)	Changma Fault	3.2	7.5	5	3.2 - 7.5 mm/yr	geology	Holocene - Late Pleistocene	Peltzer et al. 1988	149	149	149	Surface Rupture	Xu et al. (2010)	See write up and other references in write-up of event with Glenn. Peltzer et al. (1988) state their observations may not agree with those of Molnar and Deng (1984)	1	39.771	96.69
70	1	1	0	8/10/1931	Fuyun	China	SSR	7.8	8	7.9	Mw from Mo	7.00E+27	1.15E+28	8.50E+27	Molnar and Deng (1984, Figure 1):7-1.15e27 Best="measured", 8.5e27	Fuyun fault	0.1	0.52	0.3	.52 - .10	Geology	Holocene	Xu et al. (2012)	160	180	160	Surface Rupture 160 Surface Rupture 180	Shi et al. (1984); Klinger et al. (2011) Baljiinnyam et al. (1993)	Ask Weiliang for copy of Ding,G (1985) regarding seismic moment. Klinger et al. (2011) cite Calais et al. (2003) geodesy as general support that it is low-slip rate fault. Baljinnyam et al. (1993) estimate of rupture length draws on prior publications as well.	1	46.571	89.965
71	1	1	0	11/25/1930	N. Izu	Japan	SS	6.9	6.9	6.9	Mw from Mo; also Mw 6.9 from Engdahl and Villasenor (2002)	2.70E+26	3.00E+26	2.70E+26	Log Mo = 1.5M + 16.1 Wesnousky (2008): 3e26 ; Matsuda (1972): 3e26 Abe 1978: 2.7e26 wf modeling	Tanna	2	2.9	2.4	2 2 - 2.9	Geology Paleoseismology	Quaternary? Holocene	Research Group for Active Faults (1991) Kimura (2011)	28	28	28	Surface Rupture	Matsuda (1972)	Kimura (2011) reports regional GPS rate is higher(~10 mm/yr along fault and accounts for the difference by off-fault deformation.	1	35	139
72	1	1	0	1/6/1928	Laikipia	Kenya	N*	6.8	6.8	6.8	Mw from Mo	2.32E+26	2.32E+26	2.32E+26	Doser and Yarwood (1991)	Laikipia–Marmanet	0.15	0.2	0.18	.15 - .2	Geology	Pleistocene	Zielke and Strecker (2009)	38	38	38	Surface Rupture	Ambraseys (1991)	Doser and Yarwood (1991) interpret ~20 km rupture from earlier reports. Ambraseys (1991) reanalysis shows error of earlier work and reports 38 km rupture length. *Waveform modeling shows nearly pure strike-slip motion, but surface slip is strongly normal (Doser & Yarwood, 1991).	1	0.155	35.748
73	1	1	0	3/7/1927	Tango	Japan	SSL	7	7	7	Mw from Mo	4.60E+26	4.60E+26	4.60E+26	Kanamori (1973)	Gomura	0.2	0.4	0.3	0.2-0.4	Geology	Holocene, Late Pleistocene terrace offsets	Kaneda (2003)	14	35	35	Surface Rupture Geodesy - Seismology	Okada and Matsuda (1997) Kanamori (1973), (Kaneda 2003)	Surface rupture measured from slip distribution plot in Okada and Matsuda (1977). Kaneda: rupture extends into ocean.	1	35.802	134.924
74	1	1	0	3/24/1923	Luoho-Qiajiao(Daofu)	China	SSL	7.1	7.4	7.3	Mw from Mo EV02;	6.20E+26	1.35E+27	1.20E+27	Min = Pacheco and Sykes (1992): 6.2e26 from Ms conversion. Molnar and Deng (1984): use as best; range: 6 to 2.4e26*; max = 100 km, 3 m, 15 km, 3e11	Xianshuihe fault	8	16	10	10 - 20 8-16 Yu et al	Geodesy and Geolo	Holocene and Contemporary	Allen (1991) Wang et al. (2009) (InSAR) with summary citing Xu(2003) (geology) Shen et al. (2005)(geodesy) Chen et al. (2000)(geodesy) King et al. (1997)(geodesy)	60	100	80	Surface Rupture Surface Rupture	Allen et al. (1991) Papadimitriou et al. (2004), 100 km in text, reporting large displacements; Heims (1934), plate 1 fractures for 100 km., but consider some as pre-1923.	Pacheco and Sykes (1992) seismic moment is converted from Ms using Log Mo = 1.5M+16.1. Molnar and Deng (1984) is 'estimated'. Papadimitriou et al. (2004) site Heims (1934) for '100-km-long fault rupture whereas Allen also with knowledge of Heims (1934) indicates only >60 km. Allen et al. (1991) note that Heims (1934) surprising missed some critical observations. When viewing Table 3 of Papadimitriou et al. (2004) the length of rupture is assigned a 60 km value. Slip rate from Figure 1, Yu et al., 2010, at 101.2 East. Heim (1934) plate maps "fissures" over 100 km of the fault. Heims also notes that it is 6 days' travel by yak caravan to access the site.	1	30.553	101.258
75	1	1	0	12/16/1920	Haiyuan	China	SSL	7.8	8.2	8	Mw from Deng_et al.; Log Mo = 1.5M + 16.1= 8.0	6.00E+27	2.40E+28	1.20E+28	Chen and Molnar (1977): 3e28 Deng et al. (1984): 1.2e28+-factor of 2	Haiyuan	3.4	10	7	7 - 10 3.4 - 5.3 6 - 10	Geology Geology Geology	Quaternary late Pleistocene Holocene	Burchfiel et al. (1991) Li et al. (2009) Peizhen (Zhang) (1988)	200	260	237	Surface Rupture ? Surface Rupture ? Surface Rupture	Deng(1989) 237 Chen and Molnar(1977) 200 Zhang et al. (1987) 200 Burchfiel et al. (1991) 200 Deng et al. (1984) 200 BDW13: 260 Lmax	Deng et al. 1984 revise instrumental moment of Molnar and Chen, and get 1.2e28+-factor of 2. Mw from instrumental Mo.	1	36.601	105.317
76	1	1	0	10/3/1915	Pleasant Valley	Nevada	N	7.1	7.3	7.3	Mw from Mo	6.60E+26	1.03E+27	1.03E+27	Doser (1988): geologic 6.6e26 Wesnousky (2008): 10.3e26 (geologic)	Pleasant Valley (Pearce, Tobin, China Mtn, Sou Hills)	0.01	0.2	0.1	<0.2	Geology	Anderson and Machette (2000)	late Pleistocene - Quaternary	61	61	61	Surface Rupture	Wallace et al.(1984); Wesnousky (2008)		1	40.5	-117.5
77	1	1	1	1/3/1911	Chon-Kemin (Kebin)	Krygystan	R	7.9	8.1	8	Mw from Mo	8.50E+27	1.85E+28	1.35E+28	Kulikova and Kruger, 2015 wf modeling.	Kemin-Chilik and Aksu	2	10	2		geodetic*		Regional GPS compression 7-20 mm/yr across several big faults. Penultimate event, few m displacement, still visible ->2 mm/yr guestimate	169	260	177	surface rupture 159 surface rupture 180	Delvaux et al. (2001) Chen and Molnar (1977); Crosby, Arrowsmith unpublished	Delvaux et al. (2001) review prior literature and also reexamined in field for estimate of rupture length. Some ambiguity in writing: Abstract says nearly 100 km of rupture and Table 1 indicates 159 km. The 180 km value of Chen and Molnar (1977) cites others field observations and sources (e.g. Shebalin,1972) , some of which are reported in Russian. Crosby and Arrowsmith walked rupture in 2 field seasons; rupture parameters from their talks. Steve doesn't trust it.	1	43.5	77.5
78	1	1	0	4/18/1906	San Francisco	California	SSR	7.8	8	7.9	Mw from geologic Mo	7.48E+27	1.16E+28	9.62E+27	Wald et al. (1993): 4-6e27 Thatcher et al. (1997): 4-7e27 Mo from Biasi et al. 2013 L,W,D	San Andreas	16	28	21	16-28mm/yr	Geology	Holocene	Bryant and Lundberg (2002)	483	517	497	surface rupture - geodesy	Thatcher et al. (1997) range, synthesis from BWD13	Biasi et al. (2013) update length, average displacement from W08 based on later studies.	1	37.75	-122.55
79	1	1	0	7/23/1905	Bulnay	Mongolia	SSL	8.3	8.5	8.5	Mw from Mo	3.97E+28	7.67E+28	7.27E+28	Okal (1977): 5.5+-2.5e28 Schluup and Cisternas (2007):best, max 7.27e28, 7.67e28; min Mo 3.97e28 by limiting rupture depth	Bulnay Fault	2	3.1	3	4 - 16 2.0-3.1	Geology Geology	late Pleistocene- Holcene Holocene	Baljinnyam et al. (1993) Prentice et al. (2010)	350	517	375	Surface Rupture/seismology Surface Rupture	Schlupp and Cisternas (2007) Baljinnyam et al (1993) parameters from BWD2013	The slip rate reported by Baljinnyam et al. (1993) is based on climatic assumptions. Lmax includes 100 km of multi-meter offset on spur rupture not main trace	1	49	98
80	1	1	0	2/23/1892	Laguna Salada	Mexico	SSR and N	7.1	7.2	7.2	Log Mo = 1.5M + 16.1 => >7.0 Hough and Elliot (2004)	6.00E+26	8.00E+26	8.00E+26	Mueller and Rockwell (1995): >4.2e26 ; use their preferred Mw for min; Hough & Elliott for best Mw from calibrated intensity and knowledge of new InSAR	Laguna Salada and Canon Rojo	2	3	2.5	~2-3	Geology	Holocene	Mueller and Rockwell 1995	42	50	42	Surface rupture.	Mueller and Rockwell 1995; Length from Rockwell et al. (2010) SCEC poster; Lmax extrapolated, based on time to lose evidence	Oblique slip with approximately equal dip-slip and strike-slip. Moment estimate is from geology/surface slip distribution and thus a minimum because authors allow possibility of significantly longer rupture than is preserved.	1	32.4	-115.6
81	1	1	0	8/31/1896	Rikuu	Japan	R	7.2	7.4	7.2	Log Mo = 1.5M + 16.1 = 7.2, 7.4, Mw7.3 rounds down Wesnousky&Scholz, 1982 Mo	9.00E+26	1.40E+27	9.00E+26	Wesnousky et al. (1982): <1.4e27 This paper: 0.9e27, from geologic estimate	Senya	0.5	1.6	1	0.5 - 0.8 1.2 - 1.6 0.6 - 1.0	Geology Geology Geology	Holocene Holocene? Quaternary	Research Group for the Senya Fault (1986) Imaizumi et al. (1997) Kagohara et al. (2009)	37	50	40	surface rupture geodetic-surface rupture	Matsuda et al (1980) Thatcher et al. (1980)	A gap of ~8k occurs within the 37 km length of rupture. Surface rupture length value ignores parallel conjugate rupture of Kawafune fault. Thatcher et al. (1980) geodetic study extended rupture length '10 km south of the southernmost rupture segment in order to produce a minor improvement in the match of the observed and computed level changes'. The slip rate values of Imaizumi et al. (1997) and Research Group for the Senya Fault (1986) are cited by Kagohara (2009) but not examined directly by authors. Seismic moment estimate reported in Wesnousky (1982) assumes Thatcher et al.'s (1980) geodetic model (L=50 and D = 4m and dip=25°) whereas that calculated here follows more closely field measurements of Matstuda et al. (1980) (L=37 and vertical D=3.5 on 45° dipping fault)	1	39.5	140.7
82	1	1	0	10/28/1891	Nobi/ Mino-Owari	Japan	SSL	7.4	7.5	7.4	Mw from Mo Log Mo = 1.5M + 16.1=7.4	1.40E+27	2.50E+27	1.83E+27	Fukuyama et al (2007): 1.83e27; range estimated from their paper. Mikumo and Ando (1976): 1.5e27	Neodani, Nukumi, Umehara	1	2	1.6	1.0 - 1.6 ~2	Geology Geology	late Pleistocene Holocene	Kaneda and Okada (2008) Okada and Matsuda (1992)	80	80	80	Surface Rupture	Matsuda (1974)	Seismic moment of Fukuyama et al. (2007) from seismogram. Seismic moment of Mikumo and Ando (1976) calculated from geologic slip parameters reported in Matsuda (1974). Slip rate of Okada and Matsuda (1992) reported in Kaneda and Okada (2008) and not directly reexamined here.	1	35.6	136.6
83	1	1	0	9/1/1888	Canterbury	New Zealand	SSR	7	7.1	7.1	Mw = GNS current best estimate; range from length range of Khajavi et al. in press	3.80E+26	5.62E+26	6.10E+26	Khajavi et al., in press, GSAB, moment range from length range	Hope	8	17	14	8.1 - 14.5 11-17 11 - 48* 8 - 17, best 14	Geology Geology Geology Paleoseismology, LiDar	Holocene late Pleistocene late Pleistocene/Holocene Holocene	Langridge and Berryman (2010) Cowan (1991) van Dissen (1991) Unpublished new work shows the Hope fault varies along strike from 8-10 up to 18-27 mm/yr by segment. All were involved in 1888. Use middle value Khajavi et al. (in press)	40	70	65	Surface Rupture	Cowan (1991) = 30-40; length, Mw from Khajavi et al, in press.	Cowan (1991) reports dextral offsets of 1.5 and 2.6 m in fencelines crossing the Hope Fault.	1	-42.36	172.24
84	1	1	0	5/13/1887	Sonora	Mexico	N	7.2	7.2	7.2	Log Mo = 1.5M + 16.1	8.20E+26	8.20E+26	8.20E+26	This paper - see notes.	Pitaycachi, Otates, Teras	0.02	0.18	0.08	.024 .015 >.06 >.07 0.18	Geology Geology Geology Geology Geology	late Pleistocene Quaternary 23 Ma 23 Ma 23 Ma	McCalpin (1995) McCalpin (1995) Suter and Contreras (2002) p. 583, Otates, Teras Pitaycachi Suter 2008a, Teras, .08 mm/yr	86.3	101.8	101.8	surface rupture	Suter (2008); Sutur and Contreras (2002)	Length of rupture end to end is 101.4. Rupture occurred on 3 separate faults for which sum of individual fualt lengths is 86.3 km (used as min L). Seismic moment is computed here with the 86.3 km rupture length and fault parameters summarized in Table 1 of Suter and Contreras (2002) which are based on the field studies of Suter (2006, 2008ab). Using Wells and Coppersmith (), Suter and Contreras use the end to end length to estimate Mw=7.4±.3. The slip rate from Suter and Contreras (2002), accepts argument for higher rate based on geomorphology than rates in McCalpin (1995) . McCalpin (1995) is based on data reported in Bull and Pearthree (1988).	1	30.8	-109.15
85	1	1	0	3/26/1872	Owens Valley	California	SSR	7.4	7.5	7.4	Mw from Mo	1.46E+27	2.06E+27	1.62E+27	This paper - see notes. Geologic Mo from BWD13 params	Owens Valley	1	4	3.5	1-4	Geology	late Pleistocene - Holocene	Bacon Pezzopane (2007); rate from UCERF3	107	140	110	Rupture	Amos et al. 2013; Bacon and Pezzopane (2007); Beanland and Clark (1994); Values from BWD13	Amos et al. (2013) interpret 113 km rupture length as a minimum. Limits of rupture length interpreted by Bacon and Pezzopane's (2007) used here. Seismic moment calculation follows average parameters of 6±2m right-slip and 1.0±.5 normal slip summarized in Bacon and Pezzopane (2007). Range of slip rates likewise reflects Bacon and Pezzopane's summary of slip rate studies as well as their own estimate.	1	36.8	-118.16
86	1	1	0	10/21/1868	Hayward	California	SSR	6.8	7	6.9	Mw from Mo	2.30E+26	3.70E+26	3.00E+26	Yu and Segall (1996)	Hayward Fault	7.3	8.7	8	>7.3 - 8.7	Geology	Holocene	Lienkaemper et al. (2012)	50	61	61	Surface Rupture >761 Geodesy/Surface Rupture = 50-55	Lienkaemper and Williams (1999) Yu and Segall (1996)	Regarding rupture length: Slip and length are highly correlated in Yu and Segall (1996) development of geodetic model to explain earthquake, while the value of seismic moment is well resolved. Lienkaemper and Williams (1999) extend length based on trench exposure. Amount of slip in trench attributed to 1868 is poorly resolved (6 cm to 1 m).	1	37.6	-122.02
87	1	1	0	01/09/1857	Fort Tejon	California	SSR	7.8	7.9	7.8	Mw from Mo	7.12E+27	7.80E+27	7.12E+27	Zielke et al. (2010) updating Sieh (1978); max uses 3.3e11 for 3.0e11 stiffness	San Andreas	24	35	25	31 - 36.8 31.7 - 40.2	Geology Geology	Holocene late Pleistocene	Sieh and Jahns (1984) Sieh and Jahns (1984) Rate from UCERF3	360	345	339	Surface rupture	BDW2013	Sieh 1978 displacements found to often be multiples; Zielke et al., 2010; B4-Lidar evidence on rupture termination. BDW2013 updated length based on Lidar.	1	35.88	-120.5
88	1	1	0	10/16/1848	Marlborough	New Zealand	SSR	7.3	7.6	7.5	Mw from Mo	1.30E+27	3.40E+27	2.40E+27	Mason and Little (2006)	Awatere Fault	4.8	8	5.6	5.6	Geology Geology	late Pleistocene late Pleistocene 21 kyr	Little and Grapes (1998) (6-8 mm/yr) Mason et al. (2006a) (4.8-6.4 mm/yr) Benson et al. 2001 (6+-1.5)	110	160	134	Surface Rupture	Mason and Little (2006a); Little et al. (1998); max assumes 5e3 m/m taper from last displacements; nominal length tapers at 2500 m/m.	The Mason et al. slip rate is taken near southwestern end of 1848 rupture and near where there is bifurcation in fault zone? Little and Grapes values are from simpler part of fault and well within the 1848 boundary. This should be further checked. Seismic moment from geologic observations.	1	-41.48	173.42
91	0	1		11/6/1988	Gengma	China	SSR	7	7	7	GCMT	3.66E+26	3.66E+26	3.66E+26	GCMT	Lancang-Gengma Fault, Length: 70 km, Mozafarri et al. (1998)	3	3	3	3	Geology	Holocene	Ch et al. (2008) citing Allen et al. (1984)	60	60	-60	Aftershocks (EGF)	Li (1991)	Li (1991) hypothesizes that this could have been triggered by the 7.6 Lancang earthquake earlier that day. Need this paper for surface rupture: "Yu W X, Hou X Y, et al., 1991. Characteristics of surface rupture of Lancang-Gengma. J Seism Res, 14(2): 203-214"....LITERATURE INSUFFICIENT TO CLARIFY WHICH EVENTS PRODUCED WHAT SURFACE RUPTURE AS WELL AS SLIP RATE OF FAULT ON WHICH THEY OCCURRED.	0	22.83	99.72
92	0	1					SSR	7.2	7.2	7.2	Wang et al. 1992	4.5E+26	4.5E+26	4.5E+26	Chen and Wu (1989)		0	4	2	2	Geodesy,was 0-4 e	Holocene	Shen et al. (2005)	20	20	-20	Surface Ruptures	Wang et al. 1992	20 km over 4 segments that step up to 6 km	0	22.38	99.6
24	0	1		6/22/1988	Tennant Creek	Australia	R				GCMT			2.73e+25 3.46e+25 9.16e+25	GCMT	North Australian Craton		0.04	0.2	<.04	Paleoseismology	Quaternary	Crone et al. (1997)	32	32	-32	surface rupture	Crone et al. (1997).	Surface rupture generally assumed result of 3 earthquakes separated hours apart. Thus problematic how to handle correlations of individual Mw estimates to total rupture length. Slip rate approximated by dividing Crone et al's (1997) documentation of ~2m max scarp height produced during earthquake by their interpretation that "the recurrence interval of similar-size surface-rupturing earthquakes on these faults is at least severtal tens of thousands and possibly hundreds of thousands of years.	1	-19.875	133.83
50	0	1		6/16/1964	Niigata	Japan	R	7.6	7.6	7.6	Log Mo = 1.5M + 16.1	3.2E+27	3.2E+27	3.2E+27	Abe (1975)	offshore								80	80	80	aftershocks	Abe (1975)	Maybe an estimate of slip rate exists in Active Faults Book of Japan?	0	38.414	139.371
90	0	0		7/9.1905	Tsetserleg	Mongolia	SSL	7.8	8	8	Log Mo = 1.5M + 16.1= 8.3-8.5	1.1E+28	8E+28	3E+28	Okal (1977): 3-8e28 Schluup and Cisternas (2007): 1.1e28									130		>130	Surface Rupture	Schlupp and Cisternas (2007) Baljinnyam et al (1993)		0	49	99
89	0	0		12/15/1811 01/23/1811 2/07/1812	New Madrid	Missouri	R,SSR		7.2-7.3 7 7.4-7.5	7.2-7.3 7 7.4-7.5	Hough et al. (2000)			8.4E+26 3.6E+26 1.77E+28	Log Mo = 1.5M + 16.1 Log Mo = 1.5M + 16.1 Log Mo = 1.5M + 16.1	Reelfoot Fault				1.8 .0003 4.4 4.6 - 6.8 1.8 - 2.2	seismic reflection seismic reflection trenching seismic reflection	Holocene Eocene to Holocene Holocene Holocene	Van Arsdale (2000) Van Arsdale (2000) Van Arsdale (2000) Mueller et al. (1999)			60 30-40 60	seismicity seismicity/geophysics seismicity	Hough et al. (2000)	The Mw values are from isoseismal data. The interpretation and assignment of 3 shocks to each of the limbs of the New Madrid seismic zone is quite interpretive with unknown or unquantifiable uncertainites. The Holocene slip rate recorded in geology is generally over a mm/yr but orders of magnitude for periods before that (Van Arsdale (2000). It is the one true 'intra'place sequence in this data set. Geodetic data not considered here. Mw's are calculated for median value of Mw estimates.	0	35.6	-90.45

References cited in MasterEventTable_2015-10-6.xlsx

Abe, K. (1975). Re-examination of the fault model for the Niigata earthquake of 1964, Journal of Physics of Earth **23** 349-366.

Abe, K. (1975). Re-examination of the fualt model for the Niigata earthquake of 1964, Journal of Physics of Earth **23** 349-366.

Akyuz, H. S., R. Hartleb, A. Barka, E. Altunel, G. Sunal, B. Meyer, and R. Armijo (2002). Surface rupture and slip distribution of the 12 November 1999 Duzce earthquake (M 7.1), North Anatolian fault, Bolu, Turkey, B Seismol Soc Am **92** 61-66.

Allen, C. R., Z. L. Luo, H. Qian, X. Z. Wen, H. W. Zhou, and W. S. Huang (1991). Field-Study of a Highly-Active Fault Zone - the Xianshuihe Fault of Southwestern China, Geol Soc Am Bull **103** 1178-1199.

Allen, M. B., M. Kheirkhah, M. H. Emami, and S. J. Jones (2011). Right-lateral shear across Iran and kinematic change in the Arabia-Eurasia collision zone, Geophys J Int **184** 555-574.

Ambrasey.Nn (1970). Some Characteristic Features of Anatolian Fault Zone, Tectonophysics **9** 143-&.

Ambrasey.Nn, and Tchalenk.Js (1969). Dasht-E Bayaz (Iran) Earthquake of August 31, 1968 - a Field Report, B Seismol Soc Am **59** 1751-&.

Ambrasey.Nn, and A. Zatopek (1969). Mudurnu Valley West Anatolia Turkey Earthquake of 22 July 1967, B Seismol Soc Am **59** 521-&.

Ambraseys, N. N. (1991). Earthquake Hazard in the Kenya Rift - the Subukia Earthquake 1928, Geophys J Int **105** 253-269.

Amos, C. B., A. T. Lutz, A. S. Jayko, S. A. Mahan, G. B. Fisher, and J. R. Unruh (2013). Refining the Southern Extent of the 1872 Owens Valley Earthquake Rupture through Paleoseismic Investigations in the Haiwee Area, Southeastern California, B Seismol Soc Am **103** 1022-1037.

Anderson, J. G., H. Kawase, G. P. Biasi, J. N. Brune, and S. Aoi (2013). Ground Motions in the Fukushima Hamadori, Japan, Normal-Faulting Earthquake, B Seismol Soc Am **103** 1935-1951.

Anderson, J. G., S. G. Wesnousky, and M. W. Stirling (1996). Earthquake size as a function of fault slip rate, B Seismol Soc Am **86** 683-690.

Anderson, R. E., and M. N. C. Machette (2000). Fault number 1136a-d, Pleasant Valley fault zone, Pearce section, Quaternary Fault and Fold Database of the United States, ver. 1.0, U.S. Geol. Surv. Open-File Rpt. 03-417, http://qfaults.cr.usgs.gov (last accessed July 2004).

Anderson, R. S., and K. M. Menking (1994). The Quaternary Marine Terraces of Santa-Cruz, California - Evidence for Coseismic Uplift on 2 Faults, Geol Soc Am Bull **106** 649-664.

Archuleta, R. J., and S. M. Day (1980). Dynamic Rupture in a Layered Medium - the 1966 Parkfield Earthquake, B Seismol Soc Am **70** 671-689.

Arefiev, S., E. Rogozhin, R. Tatevossian, L. Rivera, and A. Cisternas (2000). The Neftegorsk (Sakhalin Island) 1995 earthquake: a rare interplate event, Geophys J Int **143** 595-607.

Armijo, R., B. Meyer, A. Hubert, and A. Barka (1999). Westward propagation of the

North Anatolian fault into the northern Aegean: Timing and kinematics, Geology **27** 267-270.

Ayele, A., and O. Kulhanek (2000). Reassessment of source parameters for the three major earthquakes in the East African rift system from historical seismograms and bulletins, Annali Di Geofisica **43** 81-94.

Ayhan, M. E., R. Burgmann, S. McClusky, O. Lenk, B. Aktug, E. Herece, and R. E. Reilinger (2001). Kinematics of the Mw=7.2, 12 November 1999, Duzce, Turkey earthquake, Geophys Res Lett **28** 367-370.

Bachmanov, D. M., V. G. Trifonov, K. T. Hessami, A. I. Kozhurin, T. P. Ivanova, E. A. Rogozhin, M. C. Hademi, and F. H. Jamali (2004). Active faults in the Zagros and central Iran, Tectonophysics **380** 221-241.

Bacon, S. N., and S. K. Pezzopane (2007). A 25,000-year record of earthquakes on the Owens Valley fault near Lone Pine, California: Implications for recurrence intervals, slip rates, and segmentation models, Geol Soc Am Bull **119** 823-847.

Bakun, W. H., M. M. Clark, R. S. Cockerham, W. L. Ellsworth, A. G. Lindh, W. H. Prescott, A. F. Shakal, and P. Spudich (1984). The 1984 Morgan-Hill, California, Earthquake, Science **225** 288-291.

Baljinnyam, I., A. Bayasgalan, B. A. Borisov, A. Cisternas, M. G. Dem'yanovich, L. Ganbaatar, V. M. Kochetkov, R. A. Kurushin, P. Molnar, H. Philip, and Y. Vaschilov (1993). Ruptures of Major Earthquakes and Active Deformation in Mongolia and Its Surroundings, Geological Society of America Memoir **181** 1-60.

Barka, A. (1996). Slip distribution along the north anatolian fault associated with the large earthquakes of the period 1939 to 1967, B Seismol Soc Am **86** 1238-1254.

Barka, A., H. S. Akyuz, E. Altunel, G. Sunal, Z. Cakir, A. Dikbas, B. Yerli, R. Armijo, B. Meyer, J. B. de Chabalier, T. Rockwell, J. R. Dolan, R. Hartleb, T. Dawson, S. Christofferson, A. Tucker, T. Fumal, R. Langridge, H. Stenner, W. Lettis, J. Bachhuber, and W. Page (2002). The surface rupture and slip distribution of the 17 August 1999 Izmit earthquake (M 7.4), North Anatolian fault, B Seismol Soc Am **92** 43-60.

Barrell, D. J. A., N. J. Litchfield, D. B. Townsend, M. Quigley, R. J. Van Dissen, R. Cosgrove, S. C. Cox, K. Furlong, P. Villamor, J. G. Begg, S. Hemmings-Sykes, R. Jongens, H. Mackenzie, D. Noble, T. Stahl, E. Bilderback, B. Duffy, H. Henham, A. Klahn, E. M. W. Lang, L. Moody, R. Nicol, K. Pedley, and A. Smith (2011). Strike-slip ground-surface rupture (Greendale Fault) associated with the 4 September 2010 Darfield earthquake, Canterbury, New Zealand, Q J Eng Geol Hydroge **44** 283-291.

Barrientos, S. E., R. S. Stein, and S. N. Ward (1987). Comparison of the 1959 Hebgen Lake, Montana and the 1983 Borah Peak, Idaho, earthquakes from geodetic observations, B Seismol Soc Am **77** 784-808.

Bawden, G. W. (2001). Source parameters for the 1952 Kern County earthquake, California: A joint inversion of leveling and triangulation observations, J Geophys Res-Sol Ea **106** 771-785.

Bayasgalan, A., J. Jackson, J. F. Ritz, and S. Carretier (1999). 'Forebergs', flower structures, and the development of large intracontinental strike-slip faults: the Gurvan Bogd fault system in Mongolia, J Struct Geol **21** 1285-1302.

Beanland, S., K. R. Berryman, and G. H. Blick (1989). Geological Investigations of the 1987 Edgecumbe Earthquake, New-Zealand, New Zeal J Geol Geop **32** 73-91.

Beanland, S., and M. Clark (1994). The Owens Valley Fault Zone, Eastern California, and surface faulting associated with the 1872 earthquake, USGS Bulletin 1982.
Beavan, J., D. Silcock, M. Hamburger, E. Ramos, C. Thibault, and R. Feir (2001). Geodetic constraints on postseismic deformation following the 1990 M-s 7.8 Luzon earthquake and implications for Luzon tectonics and Philippine Sea plate motion, Geochem Geophy Geosy **2**.
Bell, J. W., S. J. Caskey, A. R. Ramelli, and L. Guerrieri (2004). Pattern and rates of faulting in the central Nevada seismic belt, and paleoseismic evidence for prior beltlike behavior, B Seismol Soc Am **94** 1229-1254.
Bell, M. A., J. R. Elliott, and B. E. Parsons (2011). Interseismic strain accumulation across the Manyi fault (Tibet) prior to the 1997 M-w 7.6 earthquake, Geophys Res Lett **38**.
Benedetti, L., R. Finkel, G. King, R. Armijo, D. Papanastassiou, F. J. Ryerson, F. Flerit, D. Farber, and G. Stavrakakis (2003). Motion on the Kaparelli fault (Greece) prior to the 1981 earthquake sequence determined from Cl-36 cosmogenic dating, Terra Nova **15** 118-124.
Bennett, R. A., W. Rodi, and R. E. Reilinger (1996). Global positioning system constraints on fault slip rates in southern California and northern Baja, Mexico, J Geophys Res-Sol Ea **101** 21943-21960.
Berberian, M. (1979). Earthquake Faulting and Bedding Thrust Associated with the Tabas-E-Golshan (Iran) Earthquake of September 16, 1978, B Seismol Soc Am **69** 1861-1887.
Berberian, M., I. Asudeh, and S. Arshadi (1979). Surface Rupture and Mechanism of the Bob-Tangol (Southeastern Iran) Earthquake of 19 December 1977, Earth Planet Sc Lett **42** 456-462.
Berberian, M., J. A. Jackson, E. Fielding, B. E. Parsons, K. Priestley, M. Qorashi, M. Talebian, R. Walker, T. J. Wright, and C. Baker (2001). The 1998 March 14 Fandoqa earthquake (M-w 6.6) in Kerman province, southeast Iran: re-rupture of the 1981 Sirch earthquake fault, triggering of slip on adjacent thrusts and the active tectonics of the Gowk fault zone, Geophys J Int **146** 371-398.
Berberian, M., J. A. Jackson, M. Ghorashi, and M. H. Kadjar (1984). Field and Teleseismic Observations of the 1981 Golbaf Sirch Earthquakes in Se Iran, Geophys J Roy Astr S **77** 809-&.
Berberian, M., and R. Walker (2010). The Rudbar M-w 7.3 earthquake of 1990 June 20; seismotectonics, coseismic and geomorphic displacements, and historic earthquakes of the western 'High-Alborz', Iran, Geophys J Int **182** 1577-1602.
Berberian, M., and R. S. Yeats (1999). Patterns of historical earthquake rupture in the Iranian plateau, B Seismol Soc Am **89** 120-139.
Berberian, M., and R. S. Yeats (2001). Contribution of archaeological data to studies of earthquake history in the Iranian Plateau, J Struct Geol **23** 563-584.
Beroza, G. C. (1991). Near-Source Modeling of the Loma-Prieta Earthquake - Evidence for Heterogeneous Slip and Implications for Earthquake Hazard, B Seismol Soc Am **81** 1603-1621.
Blumenthal, M. (1943). Zur Geologie der Landstrecken der Erdbebeu von ende 1942 Nord-Anatolien und dortselbst ausgefurte macroseis-miche Beobachtungen, Bull. Mineral Res. Explor. lnts. Turkey **8** 33-58.

Bouchon, M. (1982). The Rupture Mechanism of the Coyote Lake Earthquake of 6 August 1979 Inferred from near-Field Data, B Seismol Soc Am **72** 745-757.
Bryant, W. A., and M. M. c. Lundberg (2002). Fault number 1b, San Andreas fault zone, North Coast section, Quaternary fault and fold database of the United States: U.S. Geological Survey website, http://earthquakes.usgs.gov/hazards/qfaults, accessed 04/30/2014 04:57 PM.
Bull, W. B., and P. A. Pearthree (1988). Frequency and Size of Quaternary Surface Ruptures of the Pitaycachi Fault, Northeastern Sonora, Mexico, B Seismol Soc Am **78** 956-978.
Burchfiel, B. C., P. Z. Zhang, Y. P. Wang, W. Q. Zhang, F. M. Song, Q. D. Deng, P. Molnar, and L. Royden (1991). Geology of the Haiyuan Fault Zone, Ningxia-Hui Autonomous Region, China, and Its Relation to the Evolution of the Northeastern Margin of the Tibetan Plateau, Tectonics **10** 1091-1110.
Burdick, L. J., and G. R. Mellman (1976). Inversion of Body Waves from Borrego Mountain Earthquake to Source Mechanism, B Seismol Soc Am **66** 1485-1499.
Caskey, S. J., S. G. Wesnousky, P. Zhang, and D. B. Slemmons (1996). Surface faulting of the 1954 Fairview Peak (M(S), 7.2) and Dixie Valley (M(S) 6.8) earthquakes, central Nevada, B Seismol Soc Am **86** 761-787.
Chatzipetros, A., S. Kokkalas, S. Pavlides, and I. Koukouvelas (2005). Palaeoseismic data and their implication for active deformation in Greece, J Geodyn **40** 170-188.
Chen, W. P., and P. Molnar (1977). Seismic Moments of Major Earthquakes and Average Rate of Slip in Central Asia, J Geophys Res **82** 2945-2969.
Chen, Z., B. C. Burchfiel, Y. Liu, R. W. King, L. H. Royden, W. Tang, E. Wang, J. Zhao, and X. Zhang (2000). Global Positioning System measurements from eastern Tibet and their implications for India/Eurasia intercontinental deformation, J Geophys Res-Sol Ea **105** 16215-16227.
Clark, M. M. (1972). Surface rupture along the Coyote Creek fault, the Borrego Mountain Earthquake of April 9, 1968, United States Geological Survey, 55-86.
Clark, M. M., A. Grantz, and M. Rubin (1972). Holocene activity of the Coyote Creek fault as recorded in sedimets of Lake Cahuilla, in *The Borrego Mountain earthquake of April 9, 1968*, U. S. Geological Survey.
Collier, R. E. L., D. Pantosti, G. D'Addezio, P. M. De Martini, E. Masana, and D. Sakellariou (1998). Paleoseismicity of the 1981 Corinth earthquake fault: Seismic contribution to extensional strain in central Greece and implications for seismic hazard, J Geophys Res-Sol Ea **103** 30001-30019.
Cowan, H. A. (1990). Late Quaternary Displacements on the Hope Fault at Glynn Wye, North Canterbury, New Zeal J Geol Geop **33** 285-293.
Cowan, H. A. (1991). The North Canterbury Earthquake of September 1, 1888, J Roy Soc New Zeal **21** 1-12.
Crone, A. J., M. N. Machette, M. G. Bonilla, J. J. Lienkaemper, K. L. Pierce, W. E. Scott, and R. C. Bucknam (1987). Surface Faulting Accompanying the Borah Peak Earthquake and Segmentation of the Lost River Fault, Central Idaho, B Seismol Soc Am **77** 739-770.
Crone, A. J., M. N. Machette, and J. R. Bowman (1997). Episodic nature of earthquake activity in stable continental regions revealed by palaeoseismicity studies of Australian and North American Quaternary faults, Aust J Earth Sci **44** 203-214.

Daligdig, J. (1997). Recent faulting and paleoseismicity along the Philippine fault zone, north central Luzon, Philippines, in *Faculty of Science*, Kyoto University.
Darby, D. J. (1989). Dislocation Modeling of the 1987 Edgecumbe Earthquake, New-Zealand, New Zeal J Geol Geop **32** 115-122.
Davis, T. L., and J. S. Namson (1994). A Balanced Cross-Section of the 1994 Northridge Earthquake, Southern California, Nature **372** 167-169.
Delvaux, D., K. E. Abdrakhmatov, and A. L. Strom (2001). Landslides and surface breaks of the 1911 Ms 8.2 Kemin earthquake, Russian Geology and Geophysics **42** 1583-1592.
Deng, Q. D., F. M. Sung, S. L. Zhu, M. L. Li, T. L. Wang, W. Q. Zhang, B. C. Burchfiel, P. Molnar, and P. Z. Zhang (1984). Active Faulting and Tectonics of the Ningxia-Hui Autonomous Region, China, J Geophys Res **89** 4427-4445.
Denham, D., L. G. Alexander, I. B. Everingham, P. J. Gregson, R. Mccaffrey, and J. R. Enever (1987). The 1979 Cadoux Earthquake and Intraplate Stress in Western-Australia, Aust J Earth Sci **34** 507-521.
Densmore, A. L., M. A. Ellis, Y. Li, R. J. Zhou, G. S. Hancock, and N. Richardson (2007). Active tectonics of the Beichuan and Pengguan faults at the eastern margin of the Tibetan Plateau, Tectonics **26**.
Dietz, L. D., and W. L. Ellsworth (1990). The October 17, 1989, Loma-Prieta, California, Earthquake and Its Aftershocks - Geometry of the Sequence from High-Resolution Locations, Geophys Res Lett **17** 1417-1420.
Djamour, Y., P. Vernant, H. R. Nankali, and F. Tavakoli (2011). NW Iran-eastern Turkey present-day kinematics: Results from the Iranian permanent GPS network, Earth Planet Sc Lett **307** 27-34.
Dolan, J. F., K. Sieh, T. K. Rockwell, P. Guptill, and G. Miller (1997). Active tectonics, paleoseismology, and seismic hazards of the Hollywood fault, northern Los Angeles basin, California, Geol Soc Am Bull **109** 1595-1616.
Dorbath, C., J. Van der Woerd, S. S. Arefiev, E. A. Rogozhin, and J. Y. Aptekman (2008). Geological and Seismological Field Observations in the Epicentral Region of the 27 September 2003 M(W) 7.2 Gorny Altay Earthquake (Russia), B Seismol Soc Am **98** 2849-2865.
Doser, D. I. (1985). Source parameters and faulting processes of the 1959 Hebgen Lake, Montana, earthquake sequence, J Geophys Res-Solid **90** 4537-4555.
Doser, D. I. (1986). Earthquake processes in the Rainbow Mountain-Fairview Peak-Dixie Valley, Nevada, region 1954-1959, J Geophys Res-Solid **91** 2572-2586.
Doser, D. I. (1988). Source Parameters of Earthquakes in the Nevada Seismic Zone, 1915-1943, J Geophys Res-Solid **93** 15001-15015.
Doser, D. I. (1990). Source characteristics of earthquakes along the southern San-Jacinto and Imperial fault zones (1937 to 1954), B Seismol Soc Am **80** 1099-1117.
Doser, D. I. (1992). Faulting processes of the 1956 San-Miguel, Baja California, earthquake sequence, Pure Appl Geophys **139** 3-16.
Doser, D. I., and D. R. Yarwood (1991). Strike-Slip Faulting in Continental Rifts - Examples from Sabukia, East-Africa (1928), and Other Regions, Tectonophysics **197** 213-224.
Dunbar, W. S., D. M. Boore, and W. Thatcher (1980). Preseismic, Coseismic and Postseismic Strain Changes Associated with the 1952 Ml = 7.2 Kern County,

California, Earthquake, B Seismol Soc Am **70** 1893-1905.
Emre, O., A. dogan, and S. Ozalp (2011b). Active Fault Map Series of Turkey, Balikesir (NJ 35-3) **Quadrangle Serial No: 4** 1:250,000.
Emre, O., A. Dogan, S. Ozalp, and C. Yildirim (2011a). Active Fault Map Series of Turkey, Bandirma (NK 35-11b), **Quadrangle, Serial NoL3** 1:250,0000.
Engdahl, E. R., and A. Vilasenor (2002). Global Seismicity: 1900 - 1999, in *International Handook of Earthqauke and Engineering Seismology* W. H. K. Lee, P. C. Kanamori and C. Kisslinger (Editors), Academic Press, 665-690.
Eyidogan, H. (1988). Rates of Crustal Deformation in Western Turkey as Deduced from Major Earthquakes, Tectonophysics **148** 83-92.
Fattahi, M., R. T. Walker, M. Talebian, R. A. Sloan, and A. Rasheedi (2014). Late Quaternary active faulting and landscape evolution in relation to the Gowk Fault in the South Golbaf Basin, SE Iran, Geomorphology **204** 334-343.
Fletcher, K. E. K., T. K. Rockwell, and W. D. Sharp (2011). Late Quaternary slip rate of the southern Elsinore fault, Southern California: Dating offset alluvial fans via Th-230/U on pedogenic carbonate, J Geophys Res-Earth **116**.
Fredrich, J., R. Mccaffrey, and D. Denham (1988). Source Parameters of 7 Large Australian Earthquakes Determined by Body Waveform Inversion, Geophysical Journal-Oxford **95** 1-13.
Fu, B. H., and Y. Awata (2007). Displacement and timing of left-lateral faulting in the Kunlun Fault Zone, northern Tibet, inferred from geologic and geomorphic features, J Asian Earth Sci **29** 253-265.
Fukuyama, E., I. Muramatu, and T. Mikumo (2007). Seismic moment of the 1891 Nobi, Japan, earthquake estimated from historical seismograms, Earth Planets Space **59** 553-559.
Gasperini, L., A. Polonia, M. N. Cagatay, G. Bortoluzzi, and V. Ferrante (2011). Geological slip rates along the North Anatolian Fault in the Marmara region, Tectonics **30**.
Genrich, J. F., Y. Bock, and R. G. Mason (1997). Crustal deformation across the Imperial Fault: Results from kinematic GPS surveys and trilateration of a densely spaced, small-aperture network, J Geophys Res-Sol Ea **102** 4985-5004.
Guo, J. M., A. M. Lin, G. Q. Sun, and J. J. Zheng (2007). Surface ruptures associated with the 1937 M 7.5 Tuosuo Lake and the 1963 M 7.0 Alake Lake earthquakes and the paleoseismicity along the Tuosuo Lake segment of the Kunlun fault, northern Tibet, B Seismol Soc Am **97** 474-496.
Haeussler, P. J., D. P. Schwartz, T. E. Dawson, H. D. Stenner, J. J. Lienkaemper, B. Sherrod, F. R. Cinti, P. Montone, P. A. Craw, A. J. Crone, and S. F. Personius (2004). Surface rupture and slip distribution of the Denali and Totschunda faults in the 3 November 2002 M 7.9 earthquake, Alaska, B Seismol Soc Am **94** S23-S52.
Haller, K. M., and R. L. c. Wheeler (1995). Fault number 601f, Lost River fault, Arco section, in Quaternary fault and fold database of the United States: , U.S. Geological Survey website, http://earthquakes.usgs.gov/hazards/qfaults, accessed 04/18/2014 12:26 PM.
Hanks, T. C., and D. P. Schwartz (1987). Morphological Dating of the Pre-1983 Fault Scarp on the Lost River Fault at Doublespring Pass Road, Custer County, Idaho, B Seismol Soc Am **77** 837-846.

Hart, E. W. (1987). Pisgah, Bulion and related faults, San Bernardino County, California, Supplement 1, CDMG Fault Evaluation Report **FER-188** 4 p.
Hartzell, S., and C. Mendoza (1991). Application of an Iterative Least-Squares Wave-Form Inversion of Strong-Motion and Teleseismic Records to the 1978 Tabas, Iran, Earthquake, B Seismol Soc Am **81** 305-331.
Hartzell, S. H., and T. H. Heaton (1983). Inversion of Strong Ground Motion and Teleseismic Waveform Data for the Fault Rupture History of the 1979 Imperial-Valley, California, Earthquake, B Seismol Soc Am **73** 1553-1583.
Hartzell, S. H., and T. H. Heaton (1986). Rupture History of the 1984 Morgan Hill, California, Earthquake from the Inversion of Strong Motion Records, B Seismol Soc Am **76** 649-674.
Harvey, T. W. (1985). Geoogy of the San Miguel falt zone, northern Baa Californnia, Mexico, in *Geology*, San Diego State University, 330.
Hauksson, E., and S. Gross (1991). Source parameters of the 1933 Long-Beach earthquake, B Seismol Soc Am **81** 81-98.
Hauksson, E., J. Stock, K. Hutton, W. Z. Yang, J. A. Vidal-Villegas, and H. Kanamori (2011). The 2010 M (w) 7.2 El Mayor-Cucapah Earthquake Sequence, Baja California, Mexico and Southernmost California, USA: Active Seismotectonics along the Mexican Pacific Margin, Pure Appl Geophys **168** 1255-1277.
Heaton, T. H. (1982). The 1971 San-Fernando Earthquake - a Double Event, B Seismol Soc Am **72** 2037-2062.
Herece, E. (1985). The fault trace of 1953 Yenice-Gonen earthquake and some examles of recent tectonic events in Biga Peninusula of northwest Turkey, in *Geology*, Penn State, 143.
Herece, E. (1990). The fault trace of the 1953 Yenice-Gonen earthquake and the westernmost known extension of the NAF system in the Biga Peninsula, Mineral Research Exploration Bulletin **111** 31-1942.
Hirabayashi, C. K., T. K. Rockwell, S. G. Wesnousky, M. W. Stirling, and F. SuarezVidal (1996). A neotectonic study of the San Miguel-Vallecitos fault, Baja California, Mexico, B Seismol Soc Am **86** 1770-1783.
Honglin, H., R. Hongliu, and Y. Ikeda (2006). Uniform strike-slip rate along the Xianshuihe-Xiaojiang fault system and its implications for active tectonics in Southeastern Tibet, Acta Geol Sin-Engl **80** 376-386.
Hough, S. E., J. G. Armbruster, L. Seeber, and J. F. Hough (2000). On the Modified Mercalli intensities and magnitudes of the 1811-1812 New Madrid earthquakes, J Geophys Res-Sol Ea **105** 23839-23864.
Hough, S. E., and A. Elliot (2004). Revisiting the 23 February 1892 Laguna Salada earthquake, B Seismol Soc Am **94** 1571-1578.
Hubert-Ferrari, A., R. Armijo, G. King, B. Meyer, and A. Barka (2002). Morphology, displacement, and slip rates along the North Anatolian Fault, Turkey, J Geophys Res-Sol Ea **107**.
Hudnut, K. W., and K. E. Sieh (1989). Behavior of the Superstition Hills Fault during the Past 330 Years, B Seismol Soc Am **79** 304-329.
Huftile, G. J., and R. S. Yeats (1996). Deformation rates across the placerita (Northridge M(w)=6.7 aftershock zone) and Hopper Canyon segments of the western transverse ranges deformation belt, B Seismol Soc Am **86** S3-S18.

IGNS (2014). New Zealand Active Fault Database, http://data. gns.cri.nz/af/.
Imaizumi, T., H. Sato, Y. Ikeda, T. Ishimaru, R. Sakai, S. Yoneda, and Y. Kubota (1997). Slip rate of the Senya fault, northeast Japan, Programme and Abstracts of Japan Association for Quaternary Research **27** 84-85 (in Japanese).
Ivashchenko, A. I., C. U. Kim, L. S. Oscorbin, L. N. Poplavskaya, A. A. Poplavsky, R. N. Burymskaya, T. G. Mikhailova, N. F. Vasilenko, and M. I. Streltsov (1997). The Neftegorsk, Sakhalin Island, earthquake of 27 May 1995, Isl Arc **6** 288-302.
Jackson, J., and D. Mckenzie (1988). The Relationship between Plate Motions and Seismic Moment Tensors, and the Rates of Active Deformation in the Mediterranean and Middle-East, Geophysical Journal-Oxford **93** 45-73.
Jackson, J. A., J. Gagnepain, G. Houseman, G. C. P. King, P. Papadimitriou, C. Soufleris, and J. Virieux (1982). Seismicity, Normal Faulting, and the Geomorphological Development of the Gulf of Corinth (Greece) - the Corinth Earthquakes of February and March 1981, Earth Planet Sc Lett **57** 377-397.
Kagohara, K., T. Ishiyama, T. Imaizumi, T. Miyauchi, H. Sato, N. Matsuta, A. Miwa, and T. Ikawa (2009). Subsurface geometry and structural evolution of the eastern margin fault zone of the Yokote basin based on seismic reflection data, northeast Japan, Tectonophysics **470** 319-328.
Kanamori, H. (1973). Mode of strain release associated with major earthquakes in Japan, Annual Review of Earth and Planetary Sciences **1** 213-239.
Kanamori, H., and J. Regan (1982). Long period surface waves, in *The imperial Valley, California earthquakeof October 15, 1979*. , Unites States Geological Survey, 15-24.
Kaneda, H. (2003). Threshold of geomorphic detectability estimated from geologic observations of active low slip-rate strike-slip faults, Geophys Res Lett **30**.
Kaneda, H., T. Nakata, H. Tsutsumi, H. Kondo, N. Sugito, Y. Awata, S. S. Akhtar, A. Majid, W. Khattak, A. A. Awan, R. S. Yeats, A. Hussain, M. Ashraf, S. G. Wesnousky, and A. B. Kausar (2008). Surface rupture of the 2005 Kashmir, Pakistan, earthquake and its active tectonic implications, B Seismol Soc Am **98** 521-557.
Kaneda, H., and A. Okada (2008). Long-term seismic behavior of a fault involved in a multiple-fault rupture: Insights from tectonic geomorphology along the Neodani fault, central Japan, B Seismol Soc Am **98** 2170-2190.
Katsumata, K., M. Kasahara, M. Ichiyanagi, M. Kikuchi, R. S. Sen, C. U. Kim, A. Ivaschenko, and R. Tatevossian (2004). The 27 May 1995 M-S 7.6 northern Sakhalin earthquake: An earthquake on an uncertain plate boundary, B Seismol Soc Am **94** 117-130.
Kelson, K. I., G. D. Simpson, W. R. Lettis, and C. C. Haraden (1996). Holocene slip rate and earthquake recurrence of the northern Calaveras fault at Leyden Creek, northern California, J Geophys Res-Sol Ea **101** 5961-5975.
Ketin, I. (1969). Uber die nordanatolische Horizontalverschiebung,, Bulletin of Mineral Research and Exploration Institute Turkey **72** 1-28.
Kimura, H., N. Ishikawa, and H. Sato (2011). Estimation of total lateral displacement including strike-slip offset and broader drag deformation on an active fault: Tectonic geomorphic and paleomagnetic evidence on the Tanna fault zone in central Japan, Tectonophysics **501** 87-97.
King, R. W., F. Shen, B. C. Burchfiel, L. H. Royden, E. C. Wang, Z. L. Chen, Y. P. Liu, X. Y. Zhang, J. X. Zhao, and Y. L. Li (1997). Geodetic measurement of crustal

motion in southwest China, Geology **25** 179-182.
Klinger, Y., M. Etchebes, P. Tapponnier, and C. Narteau (2011). Characteristic slip for five great earthquakes along the Fuyun fault in China, Nat Geosci **4** 389-392.
Kobayashi, T. (2014). Remarkable ground uplift and reverse fault ruptures for the 2013 Bohol earthquake (Mw 7.1), hilippines, reveald by SAR pixel offset analysis, Geoscience Letters **1**.
Kobayashi, T., M. Tobita, M. Koarai, T. Okatani, A. Suzuki, Y. Noguchi, M. Yamanaka, and B. Miyahara (2012). InSAR-derived crustal deformation and fault models of normal faulting earthquake (M-j 7.0) in the Fukushima-Hamadori area, Earth Planets Space **64** 1209-1221.
Kondo, H., V. Ozaksoy, and C. Yildirim (2010). Slip history of the 1944 Bolu-Gerede earthquake rupture along the North Anatolian fault system: Implications for recurrence behavior of multisegment earthquakes, J Geophys Res-Sol Ea **115**.
Kozaci, O., J. Dolan, R. Finkel, and R. Hartleb (2007). Late Holocene slip rate for the North Anatolian fault, Turkey, from cosmogenic Cl-36 geochronology: Implications for the constancy of fault loading and strain release rates, Geology **35** 867-870.
Kozaci, O., J. F. Dolan, and R. C. Finkel (2009). A late Holocene slip rate for the central North Anatolian fault, at Tahtakopru, Turkey, from cosmogenic Be-10 geochronology: Implications for fault loading and strain release rates, J Geophys Res-Sol Ea **114**.
Kurcer, A., A. Chatzipetros, S. Z. Tutkun, S. Pavlides, O. Ates, and S. Valkaniotis (2008). The Yenice-Gonen active fault (NW Turkey): Active tectonics and palaeoseismology, Tectonophysics **453** 263-275.
Kurushin, R. A. (1997). The surface rupture of the 1957 Gobi-Altay, Mongolia, earthquake, Geological Society of America **Special Paper 320** 143 p. (2 folded maps).
Langridge, R. M., and K. R. Berryman (2005). Morphology and slip rate of the Hurunui section of the Hope Fault, South Island, New Zealand, New Zeal J Geol Geop **48** 43-57.
Lasserre, C., G. Peltzer, F. Crampe, Y. Klinger, J. Van der Woerd, and P. Tapponnier (2005). Coseismic deformation of the 2001 M-w=7.8 Kokoxili earthquake in Tibet, measured by synthetic aperture radar interferometry, J Geophys Res-Sol Ea **110**.
Lewis, J. D., N. A. Daetwyler, J. A. Bunting, and J. S. Moncrief (1981). The Cadoux earthquake, Geological Survey of Western Australia Report **11**.
Li, C. Y., J. Z. Pang, and Z. Q. Zhang (2012). Characteristics, Geometry, and Segmentation of the Surface Rupture Associated with the 14 April 2010 Yushu Earthquake, Eastern Tibet, China, B Seismol Soc Am **102** 1618-1638.
Li, H. B., J. Van der Woerd, P. Tapponnier, Y. Klinger, X. X. Qi, J. S. Yang, and Y. T. Zhu (2005). Slip rate on the Kunlun fault at Hongshui Gou, and recurrence time of great events comparable to the 14/11/2001, Mw similar to 7.9 Kokoxili earthquake, Earth Planet Sc Lett **237** 285-299.
Li, Z. H., J. R. Elliott, W. P. Feng, J. A. Jackson, B. E. Parsons, and R. J. Walters (2011). The 2010 M-W 6.8 Yushu (Qinghai, China) earthquake: Constraints provided by InSAR and body wave seismology, J Geophys Res-Sol Ea **116**.
Lienkaemper, J. J., and G. Borchardt (1996). Holocene slip rate of the Hayward fault at Union City, California, J Geophys Res-Sol Ea **101** 6099-6108.

Lienkaemper, J. J., and P. L. Williams (1999). Evidence for surface rupture in 1868 on the Hayward fault in north Oakland and major rupturing in prehistoric earthquakes, Geophys Res Lett **26** 1949-1952.
Lin, A. M., T. Ouchi, A. Chen, and T. Maruyama (2001). Nature of the fault jog inferred from a deformed well in the northern Chelungpu surface rupture zone, related to the 1999 Chi-Chi, Taiwan, M-L 7.3 earthquake, B Seismol Soc Am **91** 959-965.
Lin, A. M., Z. K. Ren, D. Jia, and X. J. Wu (2009). Co-seismic thrusting rupture and slip distribution produced by the 2008 M-w 7.9 Wenchuan earthquake, China, Tectonophysics **471** 203-215.
Lindh, A. G., and D. M. Boore (1981). Control of Rupture by Fault Geometry during the 1966 Parkfield Earthquake, B Seismol Soc Am **71** 95-116.
Little, T. A., R. Grapes, and G. W. Berger (1998). Late Quaternary strike slip on the eastern part of the Awatere fault, South Island, New Zealand, Geol Soc Am Bull **110** 127-148.
Liu, H. L., and D. V. Helmberger (1983). The near-Source Ground Motion of the 6 August 1979 Coyote Lake, California, Earthquake, B Seismol Soc Am **73** 201-218.
Liu, Y., C. Xu, Z. Li, and Y. Wen (2011). Interseismic slip rate of the Garze-Yushu fault belt in the Tibetan Plateau from C-band InSAR observations between 2003 and 2010, Geophysical Research Abstracts - EGU General Assembly 2011 **13**.
Lyon-Caen, H., E. Barrier, C. Lasserre, A. Franco, I. Arzu, L. Chiquin, M. Chiquin, T. Duquesnoy, O. Flores, O. Galicia, J. Luna, E. Molina, O. Porras, J. Requena, V. Robles, J. Romero, and R. Wolf (2006). Kinematics of the North American-Caribbean-Cocos plates in Central America from new GPS measurements across the Polochic-Motagua fault system, Geophys Res Lett **33**.
Machette, M. N., A. J. Crone, and J. R. Bowman (1993). Geologic investigations of the 1986 Marryat Creek, Australia, earthquake - Implications fo paleoseismicity in stabel continental regions, U. S. Geological Survey Bulleting **2032-B** 29.
Marshall, S. T., G. J. Funning, and S. E. Owen (2013). Fault slip rates and interseismic deformation in the western Transverse Ranges, California, J Geophys Res-Sol Ea **118** 4511-4534.
Mason, D. P. M., and T. A. Little (2006). Refined slip distribution and moment magnitude of the 1848 Marlborough earthquake, Awatere Fault, New Zealand, New Zeal J Geol Geop **49** 375-382.
Mason, D. P. M., T. A. Little, and R. J. Van Dissen (2006a). Rates of active faulting during late Quaternary fluvial terrace formation at Saxton River, Awatere Fault, New Zealand, Geol Soc Am Bull **118** 1431-1446.
Matmon, A., D. P. Schwartz, P. J. Haeussler, R. Finkel, J. J. Lienkaemper, H. D. Stenner, and T. E. Dawson (2006). Denali fault slip rates and Holocene-late Pleistocene kinematics of central Alaska, Geology **34** 645-648.
Matsuda, T. (1968). Active faults and active folding (in Japanese). Symposium Research Earthquake Prediction, Tokyo 46-49
Matsuda, T. (1972). Surface faults associated with Kita-Izu Earthquake of 1930 in Izu Peninsula, Japan, in *Izu Peninsula* M. Hoshino and H. Aoki (Editors), Tokai University Press, Tokyo, 73-102.
Matsuda, T. (1974). Surface faults associated with Nobi (Mino-Owari) Earthquake of 1891, Japan, Bulletin of Earthquake Research Institute, University of Tokyo **13** 85-

126.
McCalpin, J. P. (1995). Frequency distribution of geologically determined slip rates for normal faults in the western United States, B Seismol Soc Am **85** 1867-1872.
Mccue, K. (1990). Australia Large Earthquakes and Recent Fault Scarps, J Struct Geol **12** 761-766.
Mckenzie, D. (1972). Active Tectonics of Mediterranean Region, Geophys J Roy Astr S **30** 109-185.
Meghraoui, M., and F. Doumaz (1996). Earthquake-induced flooding and paleoseismicity of the El Asnam, Algeria, fault-related fold, J Geophys Res-Sol Ea **101** 17617-17644.
Meghraoui, M., R. Jaegy, K. Lammali, and F. Albarede (1988). Late Holocene Earthquake Sequences on the El-Asnam (Algeria) Thrust-Fault, Earth Planet Sc Lett **90** 187-203.
Meriaux, A. S., K. Sieh, R. C. Finkel, C. M. Rubin, M. H. Taylor, A. J. Meltzner, and F. J. Ryerson (2009). Kinematic behavior of southern Alaska constrained by westward decreasing postglacial slip rates on the Denali Fault, Alaska, J Geophys Res-Sol Ea **114**.
Mikumo, T., and M. Ando (1976). A search into the faulting mechanism of the 1891 great Nobi earthquake, Journal of Physics of Earth **24** 63-87.
Molnar, P., and Q. D. Denq (1984). Faulting Associated with Large Earthquakes and the Average Rate of Deformation in Central and Eastern Asia, J Geophys Res **89** 6203-6227.
Mueller, K., J. Champion, M. Guccione, and K. Kelson (1999). Fault slip rates in the modern New Madrid seismic zone, Science **286** 1135-1138.
Mueller, K. J., and T. K. Rockwell (1995). Late Quaternary Activity of the Laguna-Salada Fault in Northern Baja-California, Mexico, Geol Soc Am Bull **107** 8-18.
Nairn, I. A., and S. Beanland (1989). Geological Setting of the 1987 Edgecumbe Earthquake, New-Zealand, New Zeal J Geol Geop **32** 1-13.
Nakata, T. (2014). pers. comm. (email).
Nakata, T., H. Tsutsumi, R. S. Punongbayan, R. E. Rimando, J. Daligdig, and A. Daag (1990). Surface faulting associated with the Philippine earthquake of 1990, Journal of Geography (in Japanese) **99** 95-112.
Namson, J. S., and T. L. Davis (1988). Seismically Active Fold and Thrust Belt in the San-Joaquin Valley, Central California, Geol Soc Am Bull **100** 257-273.
Okada, A. (1981). Trenches, late Holocene displacement and seismicity of the Shikano fault associated with the1943 Tottori earthquake (in Japanese with English Abstract), Kyoto Daigaku Bosai Kenkyujo Nenpo (Disaster Prevention Research Institute Annuals **24** 105-126.
Okada, A., M. Ando, and T. Tsukuda (1981). Trenches, late Holocene displace- ment and seismicity of the Shikano fault associated with the 1943 Tottori earthquake (in Japanese with English abstract), Annual Disaster Prevention Institute, Ser. B **24** 105-126.
Okada, A., and T. Matsuda (1992). Late Quaternary activity of the Neodani (Neo-Valley) fault at Midori and Naka, Neo Village, central Japan, Journal of Geography (in Japanese with English Abstract) **101** 19-37.
Okada, A., and T. Matsuda (1997). Surface faults associated with the Kita-Tango earthquake of 1927 in the northwestern part of Kinki district, central Japan, AFR

report **16** 95-135.
Okal, E. A. (1976). Surface-wave investigation of rupture mechanism of Gobi-Altai (December 4, 1957) earthquake, Phys Earth Planet In **12** 319-328.
Okal, E. A. (1977). July 9 and 23, 1905, Mongolian Earthquakes - Surface-Wave Investigation, Earth Planet Sc Lett **34** 326-331.
Oskin, M. E., J. R. Arrowsmith, A. H. Corona, A. J. Elliott, J. M. Fletcher, E. J. Fielding, P. O. Gold, J. J. G. Garcia, K. W. Hudnut, J. Liu-Zeng, and O. J. Teran (2012). Near-Field Deformation from the El Mayor-Cucapah Earthquake Revealed by Differential LIDAR, Science **335** 702-705.
Pamir, H. N., and I. H. Akyol (1943). Das Anatolische Erdbeben Ende 1939, GeoL Rundsch **32** 278-287.
Pantosti, D., R. Collier, G. DAddezio, E. Masana, and D. Sakellariou (1996). Direct geological evidence for prior earthquakes on the 1981 Corinth fault (central Greece), Geophys Res Lett **23** 3795-3798.
Peltzer, G., P. Tapponnier, Y. Gaudemer, B. Meyer, S. M. Guo, K. L. Yin, Z. T. Chen, and H. G. Dai (1988). Offsets of late Quaternary morphology, rate of slip, and recurrence of large earthquakes on the Chang Ma fault (Gansu, China), J Geophys Res-Solid **93** 7793-7812.
Pettinga, J., M. D. Yetton, R. J. Van Dissen, and G. Downes (2001). Earthquake source identification and characterisation for the Canterbury Region, South Island, New Zealand, Bulltin of the New Zealand Society for Earthquake Engineering **34** 282-317.
Pinar, A., Y. Honkura, and M. Kikuchi (1996). A rupture model for the 1967 Mudurnu Valley, Turkey earthquake and its implication for seismotectonics in the western part of the North Anatolian Fault Zone, Geophys Res Lett **23** 29-32.
Plafker, G. (1976). Tectonic Aspects of Guatemala Earthquake of 4 February 1976, Science **193** 1201-1208.
Polonia, A., L. Gasperini, A. Amorosi, E. Bonatti, G. Bortoluzzi, N. Cagatay, L. Capotondi, M. H. Cormier, N. Gorur, C. McHugh, and L. Seeber (2004). Holocene slip rate of the North Anatolian Fault beneath the Sea of Marmara, Earth Planet Sc Lett **227** 411-426.
Prentice, C. S., M. Rizza, and J. R. Ritz (2010). The Bogd and Bulnay Faults of Mongolia: Slip Rate and Earthquake Recurrence Along Two Intracontinental Strike-Slip Faults (Invited), in *American Geophysical Union*, San Francisco, abstract #T42A-08.
Proctor, R. J., R. Crook, M. H. Mckeown, and R. L. Moresco (1972). Relation of Known Faults to Surface Ruptures, 1971 San-Fernando Earthquake, Southern-California, Geol Soc Am Bull **83** 1601-&.
Pucci, S., P. M. De Martini, and D. Pantosti (2008). Preliminary slip rate estimates for the Duzce segment of the North Anatolian Fault Zone from offset geomorphic markers, Geomorphology **97** 538-554.
Reasenberg, P., and W. L. Ellsworth (1982). Aftershocks of the Coyote Lake, California, Earthquake of August 6, 1979 - a Detailed Study, J Geophys Res **87** 637-655.
Research-Group-for-Active-Faults (1991). Active faults in Japan: sheet maps and inventories, University of Tokyo Press, Tokyo.
Research-Group-for-the-Senya-Fault (1986). Holocene activities and near-surface features of the Senya fault, Akita prefecture, Japan - Excavation study at Komori,

Senhata-cho, Bulletin of Earthquake Research Institute, University of Tokyo **61** 339-402 (in Japanese with English abstract).
Ritz, J. F., E. T. Brown, D. L. Bourles, H. Philip, A. Schlupp, G. M. Raisbeck, F. Yiou, and B. Enkhtuvshin (1995). Slip rates along active faults estimated with cosmic-ray-exposure dates - application to the Bogd fault, Gobi-Altai, Mongolia, Geology **23** 1019-1022.
Rizza, M., J. F. Ritz, R. Braucher, R. Vassallo, C. Prentice, S. Mahan, S. McGill, A. Chauvet, S. Marco, M. Todbileg, S. Demberel, and D. Bourles (2011). Slip rate and slip magnitudes of past earthquakes along the Bogd left-lateral strike-slip fault (Mongolia), Geophys J Int **186** 897-927.
Rockwell, P. a. (1995). Late Holocene slip rate for the Coyote Creek fault, Imperial County, California, Geol Soc Am Bull **Abstracts with Programs 27** p. 72.
Rogozhin, E. A., A. N. Ovsyuchenko, A. V. Marakhanov, and E. A. Ushanova (2007). Tectonic setting and geological manifestations of the 2003 Altai earthquake, Geotectonics+ **41** 87-104.
Schlupp, A., and A. Cisternas (2007). Source history of the 1905 great Mongolian earthquakes (Tsetserleg, Bolnay), Geophys J Int **169** 1115-1131.
Schwartz, D. P., L. S. Cluff, and T. W. Donnelly (1979). Quaternary Faulting Along the Caribbean-North-American Plate Boundary in Central-America, Tectonophysics **52** 431-445.
Segall, P., and Y. J. Du (1993). How Similar Were the 1934 and 1966 Parkfield Earthquakes, J Geophys Res-Sol Ea **98** 4527-4538.
Sharp, R. V. (1981). Variable Rates of Late Quaternary Strike Slip on the San-Jacinto Fault Zone, Southern-California, J Geophys Res **86** 1754-1762.
Sharp, R. V., K. E. Budding, J. Boatwright, M. J. Ader, M. G. Bonilla, M. M. Clark, T. E. Fumal, K. K. Harms, J. J. Lienkaemper, D. M. Morton, B. J. Oneill, C. L. Ostergren, D. J. Ponti, M. J. Rymer, J. L. Saxton, and J. D. Sims (1989). Surface Faulting Along the Superstition Hills Fault Zone and Nearby Faults Associated with the Earthquakes of 24 November 1987, B Seismol Soc Am **79** 252-281.
Shen, Z. K., J. N. Lu, M. Wang, and R. Burgmann (2005). Contemporary crustal deformation around the southeast borderland of the Tibetan Plateau, J Geophys Res-Sol Ea **110**.
Shi, J., X. Feng, S. Ge, Z. Q. Yang, M. bo, and J. Hu (1984). The Fuyun earthqake fault zone in Xianhiang, China, A collection of papers of International Symposium on Continental Seismicity and Earthquake Prediction (ISCSEP) 325-346.
Sieh, K. E. (1978). Slip along San-Andreas fault associated with great 1857 earthquake, B Seismol Soc Am **68** 1421-&.
Sieh, K. E., and R. H. Jahns (1984). Holocene Activity of the San-Andreas Fault at Wallace-Creek, California, Geol Soc Am Bull **95** 883-896.
Simoes, M., J. P. Avouac, and Y. G. Chen (2007). Slip rates on the Chelungpu and Chushiang thrust faults inferred from a deformed strath terrace along the Dungpuna river, west central Taiwan, J Geophys Res-Sol Ea **112**.
Simpson, G. D., J. N. Baldwin, K. I. Kelson, and W. R. Lettis (1999). Late holocene slip rate and earthquake history for the northern Calaveras fault at Welch Creek, eastern San Francisco Bay area, California, B Seismol Soc Am **89** 1250-1263.
Stein, R. S. (1981). Seismic and Aseismic Deformation Associated with the 1952 Kern

County, California, Earthquake and Relationship to the Quaternary History of the White Wolf Fault, J Geophys Res **86** 4913-4928.
Stein, R. S., and G. Ekstrom (1992). Seismicity and Geometry of a 110-Km-Long Blind Thrust-Fault .2. Synthesis of the 1982-1985 California Earthquake Sequence, J Geophys Res-Sol Ea **97** 4865-4883.
Stein, R. S., and G. C. P. King (1984). Seismic Potential Revealed by Surface Folding - 1983 Coalinga, California, Earthquake, Science **224** 869-872.
Suter, M. (2006). Contemporary studies of the 3 May 1887 M-W 7.5 Sonora, Mexico (Basin and Range province) earthquake, Seismol Res Lett **77** 134-147.
Suter, M. (2008). Structural Configuration of the Otates Fault (Southern Basin and Range Province) and Its Rupture in the 3 May 1887 M(W) 7.5 Sonora, Mexico, Earthquake, B Seismol Soc Am **98** 2879-2893.
Suter, M. (2008). Structural configuration of the Teras fault (southern Basin and Range Province) and its rupture in the 3 May 1887 M(W) 7.5 Sonora, Mexico earthquake, Rev Mex Cienc Geol **25** 179-195.
Suter, M., and J. Contreras (2002). Active tectonics of northeastern Sonora, Mexico (southern Basin and Range province) and the 3 May 1887 M-w 7.4 earthquake, B Seismol Soc Am **92** 581-589.
Swan, F. H. (1988). Temporal Clustering of Paleoseismic Events on the Oued Fodda Fault, Algeria, Geology **16** 1092-1095.
Tang, R. (1984). On the seismogeological setting and conditions of seismogenic structures of 1981 Daofu earthquake, Seismology and Geology (Di Zhin di Zhi) (in Chinese) **6** 33-40.
Tatar, O., F. Poyraz, H. Gursoy, Z. Cakir, S. Ergintav, Z. Akpinar, F. Kocbulut, F. Sezen, T. Turk, K. O. Hastaoglu, A. Polat, B. L. Mesci, O. Gursoy, I. E. Ayazli, R. Cakmak, A. Belgen, and H. Yavasoglu (2012). Crustal deformation and kinematics of the Eastern Part of the North Anatolian Fault Zone (Turkey) from GPS measurements, Tectonophysics **518** 55-62.
Thatcher, W., G. Marshall, and M. Lisowski (1997). Resolution of fault slip along the 470-km-long rupture of the great 1906 San Francisco earthquake and its implications, J Geophys Res-Sol Ea **102** 5353-5367.
Thatcher, W., T. Matsuda, T. Kato, and J. B. Rundle (1980). Lithospheric Loading by the 1896 Riku-U Earthquake, Northern Japan - Implications for Plate Flexure and Asthenospheric Rheology, J Geophys Res **85** 6429-6435.
Thomas, A. P., and T. K. Rockwell (1996). A 300- to 550-year history of slip on the Imperial fault near the US-Mexico border: Missing slip at the Imperial fault bottleneck, J Geophys Res-Sol Ea **101** 5987-5997.
Toke, N. A., J. R. Arrowsmith, M. J. Rymer, A. Landgraf, D. E. Haddad, M. Busch, J. Coyan, and A. Hannah (2011). Late Holocene slip rate of the San Andreas fault and its accommodation by creep and moderate-magnitude earthquakes at Parkfield, California, Geology **39** 243-246.
Treiman, J., and M. M. c. Lundberg (1999). Fault number 125e, San Jacinto fault, Borrego Mountain section, Quaternary fault and fold database of the United States: U.S. Geological Survey website, http://earthquakes.usgs.gov/hazards/qfaults, accessed 04/27/2014 10:01 AM.
Treiman, J., and M. M. c. Lundberg (1999). Fault Numer 127c, Newport-Inglewood-Rose

Canyon fault zone, Dana Point section,, Quaternary fault and fold database of the United States: U.S. Geological Survey website, http://earthquakes.usgs.gov/hazards/qfaults, accessed 04/29/2014 03:34 AM.
Treiman, J. A., K. J. Kendrick, W. A. Bryant, T. K. Rockwell, and S. F. McGill (2002). Primary surface rupture associated with the M-w 7.1 16 October 1999 Hector Mine earthquake, San Bernardino County, California, B Seismol Soc Am **92** 1171-1191.
Treiman, J. J. (2003). Fault number 122a, Pisgah-Bullion fault zone, Pisgah section., in Quaternary fault and fld database of the United States, U.S. Geological Survey website, http://earthquakes.usgs.gov/hazards/qfaults.
Treiman, J. J. c. (2000). Fault numbers 105b and 105h, Sierra Madre fault zone, San Fernando section, in Quaternary fault and fold database of the United States, U.S. Geological Survey website, http://earthquakes.usgs.gov/hazards/qfaults, accessed 04/26/2014 05:07 PM.
Trifunac, M. D. (1972). Tectonic Stress and Source Mechanism of Imperial Valley, California, Earthquake of 1940, B Seismol Soc Am **62** 1283-&.
Tsutsumi, H. (2014). email communication.
Tsutsumi, H., A. I. Kozhurin, M. I. Strel'tsov, T. Ueki, Y. Suzuki, and M. Watanabe (2000). Active faults and paleoseismoogy in northeastern Sakhalin, Russia, Journal of Geography (in Japanese with English Abstract) **109** 294-301.
Tsutsumi, H., Y. Suzuki, A. I. Kozhurin, M. I. Strel'tsov, T. Ueki, H. Goto, K. Okumura, R. F. Bulgakov, and H. Kitagawa (2005). Late Quaternary faulting along the western margin of the Poronaysk Lowland in central Sakhalin, Russia, Tectonophysics **407** 257-268.
Ucarkus, G., Z. Cakir, and R. Armijo (2011). Western Termination of the Mw 7.4, 1999 Izmit Earthquake Rupture: Implications for the Expected Large Earthquake in the Sea of Marmara, Turk J Earth Sci **20** 379-394.
Uemura, Y. (1994). Fault topography along the Gomura fault system (in Japanese), in Surface Faults Associated With the Kita-Tango Earthquake of 1927 and Active Tectonics Around the Tango Peninsula, Fault Research Data Center, Osaka.
Van der Woerd, J., F. J. Ryerson, P. Tapponnier, A. S. Meriaux, Y. Gaudemer, B. Meyer, R. C. Finkel, M. W. Caffee, G. G. Zhao, and Z. Q. Xu (2000). Uniform Slip-Rate along the Kunlun Fault: Implications for seismic behaviour and large-scale tectonics, Geophys Res Lett **27** 2353-2356.
Van Der Woerd, J., P. Tapponnier, F. J. Ryerson, A. S. Meriaux, B. Meyer, Y. Gaudemer, R. C. Finkel, M. W. Caffee, G. G. Zhao, and Z. Q. Xu (2002). Uniform postglacial slip-rate along the central 600 km of the Kunlun Fault (Tibet), from Al-26, Be-10, and C-14 dating of riser offsets, and climatic origin of the regional morphology, Geophys J Int **148** 356-388.
VanArsdale, R. (2000). Displacement history and slip rate on the Reelfoot fault of the New Madrid seismic zone, Eng Geol **55** 219-226.
Vandissen, R., and R. S. Yeats (1991). Hope Fault, Jordan Thrust, and Uplift of the Seaward Kaikoura Range, New-Zealand, Geology **19** 393-396.
Vernant, P., F. Nilforoushan, D. Hatzfeld, M. R. Abbassi, C. Vigny, F. Masson, H. Nankali, J. Martinod, A. Ashtiani, R. Bayer, F. Tavakoli, and J. Chery (2004). Present-day crustal deformation and plate kinematics in the Middle East constrained by GPS measurements in Iran and northern Oman, Geophys J Int **157** 381-398.

Villamor, P., N. Litchfield, D. Barrell, R. Van Dissen, S. Hornblow, M. Quigley, S. Levick, W. Ries, B. Duffy, J. Begg, D. Townsend, T. Stahl, E. Bilderback, D. Noble, K. Furlong, and H. Grant (2012). Map of the 2010 Greendale Fault surface rupture, Canterbury, New Zealand: application to land use planning, New Zeal J Geol Geop **55** 223-230.

Wakabayashi, J., and D. L. Smith (1994). Evaluation of Recurrence Intervals, Characteristic Earthquakes, and Slip Rates Associated with Thrusting Along the Coast Range Central Valley Geomorphic Boundary, California, B Seismol Soc Am **84** 1960-1970.

Wald, D. J., H. Kanamori, D. V. Helmberger, and T. H. Heaton (1993). Source Study of the 1906 San-Francisco Earthquake, B Seismol Soc Am **83** 981-1019.

Walker, R. (2014). Email communication of March 8, 2014 S. G. Wesnousky (Editor).

Walker, R., and J. Jackson (2002). Offset and evolution of the Gowk fault, SE Iran: a major intra-continental strike-slip system, J Struct Geol **24** 1677-1698.

Walker, R., J. Jackson, and C. Baker (2004). Active faulting and seismicity of the Dasht-e-Bayaz region, eastern Iran, Geophys J Int **157** 265-282.

Walker, R. T., M. M. Khatib, A. Bahroudi, A. Rodes, C. Schnabel, M. Fattahi, M. Talebian, and E. Bergman (2013). Co-seismic, geomorphic, and geologic fold growth associated with the 1978 Tabas-e-Golshan earthquake fault in eastern Iran,, Geomorphology **http://dx.doi.org/10.1016/j.geomorph.2013.02.016** in press - published on line.

Wallace, L. M., J. Beavan, R. McCaffrey, K. Berryman, and P. Denys (2007). Balancing the plate motion budget in the South Island, New Zealand using GPS, geological and seismological data, Geophys J Int **168** 332-352.

Wallace, R. E. (1980). Map of fault scarps formed during earthquake of October 2, 1915, Pleasant Valley, Nevada, and other young fault scarps, in *U.S. Geological Survey Open File Report*, U. S. Geological Survey, Reston, VA.

Wang, H., T. J. Wright, and J. Biggs (2009). Interseismic slip rate of the northwestern Xianshuihe fault from InSAR data, Geophys Res Lett **36**.

Wang, H., C. J. Xu, and L. L. Ge (2007). Coseismic deformation and slip distribution of the 1997 M-w 7.5 Manyi, Tibet, earthquake from InSAR measurements, J Geodyn **44** 200-212.

Wang, Q., P. Z. Zhang, J. T. Freymueller, R. Bilham, K. M. Larson, X. Lai, X. Z. You, Z. J. Niu, J. C. Wu, Y. X. Li, J. N. Liu, Z. Q. Yang, and Q. Z. Chen (2001). Present-day crustal deformation in China constrained by global positioning system measurements, Science **294** 574-577.

Wang, S. F., W. Erchie, X. M. Fang, and B. Fu (2008). Late cenozoic systematic left-lateral stream deflections along the Ganzi-Yushu fault, Xianshuihe fault system, eastern Tibet, Int Geol Rev **50** 624-635.

Wang, Y., E. Wang, Z. Shen, M. Wang, W. Gan, X. Qiao, G. Meng, T. Li, W. Tao, Y. ang, J. Cheng, and L. Peng (2008). GPS-constrained inversion of present day slip rates along major faults of the Sichuan-Yunnan region, China, Science in China (Series D) **51** 1267-1283.

Wells, D. L., and K. J. Coppersmith (1994). New empirical relationships among magnitude, rupture length, rupture width, rupture area, and surface displacement, B Seismol Soc Am **84** 974-1002.

Wen, X., X. XU, R. Zheng, Y. Xie, and C. Wan (2003). Average slip-rate and recent large earthquake ruptures along the Garze-Yush fault, Science in China (Series D) **46 Supplement** 276-288.

Wen, Y. Y., and K. F. Ma (2010). Fault geometry and distribution of asperities of the 1997 Manyi, China (Mw=7.5), earthquake: Integrated analysis from seismological and InSAR data, Geophys Res Lett **37**.

Wesnousky, S. G. (2008). Displacement and geometrical characteristics of earthquake surface ruptures: Issues and implications for seismic-hazard analysis and the process of earthquake rupture, B Seismol Soc Am **98** 1609-1632.

Wesnousky, S. G., C. H. Scholz, and K. Shimazaki (1982). Deformation of an Island-Arc - Rates of Moment Release and Crustal Shortening in Intraplate Japan Determined from Seismicity and Quaternary Fault Data, J Geophys Res **87** 6829-6852.

Witkind, I. J. (1964). Reactivated faults north of Hebgen Lake, U. S. Geological Survey **Professional Paper 435-G** 37-50.

Xu, X. (2003). Pattern of latest tectonic motion and its dynamics for active blocks in Sichuan-Yunan region China (in Chinese), Science in China (Series D) **33** 151-162.

Xu, X., R. S. Yeats, and G. Yu (2010). Five Short Historical Earthquake Surface Ruptures near the Silk Road, Gansu Province, China, B Seismol Soc Am **100** 541-561.

Xu, X.-w., X.-z. Sun, X.-b. Tan, K. Li, G.-h. Yu, M. Etchbes, Y. Klinger, P. Tapponnier, and J. van der Woerd (2012). Fuyun fault: Long-term faulting behavior under low crustal strain rate, Seismology and Geology (Di zhen di zhi) **34** 606-617.

Xu, X. W., G. H. Yu, Y. Klinger, P. Tapponnier, and J. Van der Woerd (2006). Reevaluation of surface rupture parameters and faulting segmentation of the 2001 Kunlunshan earthquake (M(w)7.8), northern Tibetan Plateau, China, J Geophys Res-Sol Ea **111**.

Yielding, G., J. A. Jackson, G. C. P. King, H. Sinvhal, C. Vitafinzi, and R. M. Wood (1981). Relations between Surface Deformation, Fault Geometry, Seismicity, and Rupture Characteristics during the El-Asnam (Algeria) Earthquake of 10 October 1980, Earth Planet Sc Lett **56** 287-304.

Yu, E., and P. Segall (1996). Slip in the 1868 Hayward earthquake from the analysis of historical triangulation data, J Geophys Res-Sol Ea **101** 16101-16118.

Zhang, P. Z. (2013). Beware of slowly slipping faults, Nat Geosci **6** 323-324.

Zhou, H. L., C. R. Allen, and H. Kanamori (1983). Rupture Complexity of the 1970 Tonghai and 1973 Luhuo Earthquakes, China, from P-Wave Inversion, and Relationship to Surface Faulting, B Seismol Soc Am **73** 1585-1597.

Zhu, C. (1985). Qujiang fault activity in Quaternary period (in Chinese with English Abstract), China Academic Journal Electronic Publishing House **Provided by Wei Liang**.

Zielke, O., and M. R. Strecker (2009). Recurrence of Large Earthquakes in Magmatic Continental Rifts: Insights from a Paleoseismic Study along the Laikipia-Marmanet Fault, Subukia Valley, Kenya Rift, B Seismol Soc Am **99** 61-70.